Tutorial. Surface EMG detection in space and time: Best practices

Journal of Electromyography and Kinesiology 49 (2019) 102363

Contents lists available at ScienceDirect

Journal of Electromyography and Kinesiology

journal homepage: www.elsevier.com/locate/jelekin

Tutorial. Surface EMG detection in space and time: Best practices

R. Merletti[a,*], S. Muceli[b,c]

[a] LISiN, Dept. of Electronics and Telecommunications, Politecnico di Torino, Italy
[b] Division of Signal Processing and Biomedical Engineering, Department of Electrical Engineering, Chalmers University of Technology, Gothenburg, Sweden
[c] Imperial College, London, UK

ARTICLE INFO

Keywords:
Tutorial
Teaching
surface EMG
High Density sEMG
Multichannel array sEMG
Physiotherapists
Kinesiologists
Movement scientists

ABSTRACT

This tutorial is aimed to non-engineers using, or planning to use, surface electromyography (sEMG) as an assessment tool in the prevention, monitoring and rehabilitation fields. Its first purpose is to address the issues related to the origin and nature of the signal and to its detection (electrode size, distance, location) by one-dimensional (bipolar and linear arrays) and two-dimensional (grids) electrode systems while avoiding advanced mathematical, physical or physiological issues. Its second purpose is to outline best practices and provide general guidelines for proper signal detection. Issues related to the electrode-skin interface, signal conditioning and interpretation will be discussed in subsequent tutorials.

1. Introduction

In the last decades, the applications of surface EMG (sEMG) have grown in the traditional fields (sport, movement and gait analysis) as well as in novel ones (obstetrics, occupational and art medicine, aging, veterinary medicine, rehabilitation and gaming) while the focus expanded from neurophysiological research to neurorehabilitation, preventive medicine, ergonomics, and assessment of interventions. This growth led to the publication of (a) six textbooks, (b) over 90 journal reviews, (c) European Recommenda-tions (Barbero et al., 2012; Hermens et al., 1999, 2000; Merletti and Farina, 2016) and (d) on-line material on a few teaching and encyclopaedia websites (https://www.robertomerletti.it, https://www.lisin.polito.it, https://en.wikipedia.org/wiki/Electromyography, https://onlinelibrary.wiley.com/doi/10.1002/047134608X.W1413, https://www.sciencedirect.com/science/article/pii/B9780128012383999872).

The transfer of knowledge from biomedical engineering and clinical research laboratories to schools and health delivery institutions is lagging and is very heterogeneous from country to country. Only a few European schools in movement sciences, rehabilitation sciences and physiotherapy offer courses in the field. Very few private practitioners and physiotherapists working in rehabilitation centers are familiar with the sEMG techniques. This is in contrast to the training of cardiologists in electrocardiography (ECG) and of neurologists in electroencephalography (EEG) which has taken place for 70 years. With respect to these bioelectric signals, sEMG has, at this time, limited diagnostic power but is a powerful tool for prevention, assessment and evaluation of effectiveness of treatments and interventions as described in chapters 12–20 of (Merletti and Farina, 2016) and website https://www.robertomerletti.it.

This tutorial is aimed to clinical scientists and rehabilitation operators and has the objective of reducing the gap between basic sEMG technology and its clinical application by providing a technical overview of fundamental sEMG concepts, methods and recommendations for best practices, without addressing advanced mathematical, physical or physiological issues. In particular, it focuses on recent applications of High Density sEMG. We provide a set of recommendations for best practice when recording and analyzing sEMG signals. We also provide the rationale leading to each of those recommendations. In an effort to making a tutorial useful to sEMG users with different backgrounds, we did not report any mathematical formulation. Few sections may require basic knowledge in neuromuscular anatomy, electrophysiology, and signal processing. However, when this is the case, we provide references for the reader interested in further investigating the topic.

Abbreviations: AP, action potential generated by a single fiber and described in time or space; CV, conduction velocity of the MUAPs; DD, double differential; ECG, electrocardiogram/electrocardiography; EEG, electroencephalogram/electroencephalography; EMG, electromyogram/electromyography; IED, inter-electrode distance (center to center); MU, motor unit; MUAP, motor unit action potential; NMJ, neuromuscular junction; RMS, root mean square value; SD, single differential; sEMG, surface electromyogram; TS, tendon spread: spread of the fiber-tendon junctions of a MU; VL, vastus lateralis muscle; VM, Vastus medialis muscle

* Corresponding author.
E-mail addresses: roberto.merletti@formerfaculty.polito.it (R. Merletti), muceli@chalmers.se (S. Muceli).

https://doi.org/10.1016/j.jelekin.2019.102363
Received 10 June 2019; Received in revised form 26 August 2019; Accepted 3 October 2019

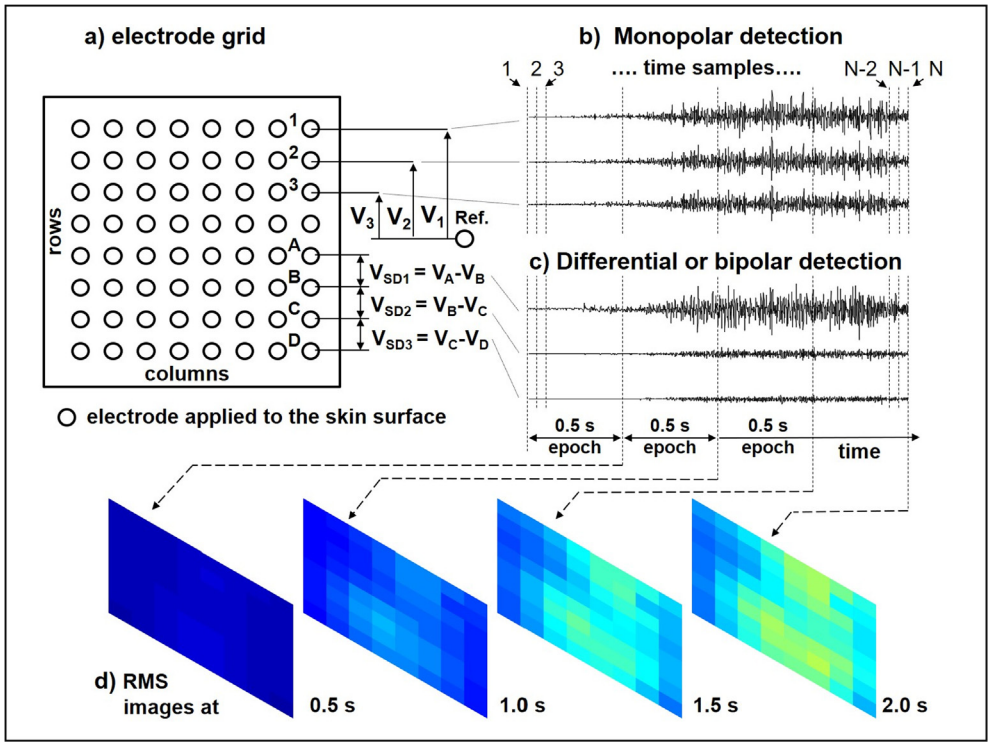

Fig.1. Surface EMG signals in space and time. (a) Schematic representation of an electrode grid of 8 rows by 8 columns applied over a muscle, (b) examples of three monopolar signals V_1 to V_3 versus time, from electrodes 1, 2, 3, measured with respect to a reference electrode, placed on an electrically inactive region, (c) examples of differential ($V_A - V_B$ to $V_C - V_D$) signals versus time. The 1, 2, 3, …, N − 1, N dashed vertical lines represent N samples of these signals in time (for clarity the samples in time are much further apart than in real conditions). Each time sample provides a map of the distribution in space. Examples of movies of instantaneous maps are available at https://www.robertomerletti.it/en/emg/material/videos/f1/to/f4/. (d) Each electrode (or pair of electrodes) provides a sample in space, which is a signal evolving in time, defining a pixel in the image. Signal features, such as the root mean square value (RMS) of each signal (pixel) may be computed over specific time intervals (time epochs or time windows or simply "epochs"). In panel d, RMS maps are monopolar with epoch = 0.5 s. Examples of movies of RMS maps are available at https://www.robertomerletti.it/en/emg/material/videos/f5/to/f19/.

2. The EMG as a signal distribution in space, which is evolving in time: The analog EMG "movie"

2.1. Generation of the signal distribution in space and time

The instantaneous surface EMG (sEMG) is a two-dimensional (2D) distribution (instantaneous map) of electric potential (that is voltage) over the surface of the skin, like the ECG on the chest or the EEG on the scalp. This potential distribution is an analog (continuous) "electrical image" or "map" evolving in time, as a movie. This 2D analog signal is sampled in space (by the electrodes, as described in Section 3.1) and in time (by an electronic sampler) providing a sequence of sampled time frames. An example is depicted in Fig. 1a where one frame is divided into pixels corresponding to the electrodes of a 2D electrode array whose signals, evolving in time, can be detected using the monopolar or single differential (SD, bipolar) technique, as indicated in Fig. 1b and c where each dashed line represents a frame (N frames are indicated). Colors may be used to represent the instantaneous potential amplitude distribution, which is evolving in time. The number of electrodes may range from two (one detection electrode and one reference electrode in the single channel monopolar system) to hundreds, as in High Density sEMG (or Multichannel Array sEMG) leading to a 3D sEMG imaging with two dimensions in space and one in time (Urbanek and van der Smagt, 2016).

The generators of these time-evolving maps of surface electrical potential are the motor unit action potentials (MUAP) of the active motor units (MU), which comprise the thousands of action potentials (AP) generated by the individual fibers of such MUs in the muscle. The AP generation mechanism is presumed known to the reader, is described in any textbook of biophysics or neurophysiology (e.g. Malmivuo and Plonsey, 1995) and shortly summarized here. The neuromuscular junction (NMJ) is the synapse between each axonal branch of a motor neuron and the muscle fiber it innervates. When acetylcholine is released at the NMJ, two depolarized regions are generated and propagate toward the fiber-tendon junctions at a velocity of about 4 m/s (normal range of 3–5 m/s) as indicated in Fig. 2a. Each depolarized region has three sub-regions where current flows in or out of the membrane, as indicated in gray in Fig. 2a and in the current profiles in Fig. 2b. As a first approximation, these currents are modeled as two current tripoles propagating in opposite directions, as indicated in Fig. 2b. These currents flow in the conductive medium and generate the electrical potential distribution on the skin surface (Rosenfalck, 1969; Gootzen, 1990; Merletti et al., 1999a,b; Stegeman et al., 2000). Although more accurate models are now available (Farina and Merletti, 2001a; Lowery et al., 2002; Mesin and Farina, 2004), the early tripole model provides examples that are simpler and easier to understand.

A α-motoneurone and the muscle fibers it innervates form a MU, whose fibers are activated together at each discharge of the motor neuron, and generate a propagating MUAP, which is the algebraic summation (in space and time) of the APs generated by the individual fibers of that MU. Dozens to hundreds of motor neurons are activated at average discharge rates ranging from 5–6 pulses/s to 30–40 pulses/s, depending on the required force and the contraction speed. The resulting signals are MUAP trains whose algebraic sum in each point on the skin above and near the muscle is the interferential monopolar sEMG signal at that specific point, versus time, measured with respect to a reference electrode, as indicated in Fig. 1a. Differential measurements are obtained by taking the difference between two adjacent monopolar signals as indicated in Fig. 1a, usually, but not necessarily, in the direction of the MUAP propagation, that is the direction of the muscle fibers. The monopolar (or differential) sEMG signal is the summation of many MUAPs and, for muscle contractions above 40–50% of the maximal voluntary contraction its probability density function approximates a Gaussian distribution (Clancy and Hogan, 1999; Nazarpour et al., 2013).

The electrodes, depicted as circles, in Fig. 1a perform a sampling in space of each instantaneous analog sEMG "map". The vertical dashed lines in Fig. 1b and c represent the sampling in time of the sEMG signals. Each dashed line corresponds to an *instantaneous map,* that is to a frame of a "movie" describing the spatial distribution of sEMG (sample by sample) that will be described in Section 3. A sEMG "feature" is computed over specific intervals (time epochs or time windows) for each channel, generating a sequence of *feature maps*. Fig. 1d depicts four sequential "RMS maps", each computed over a 0.5 s epoch. The

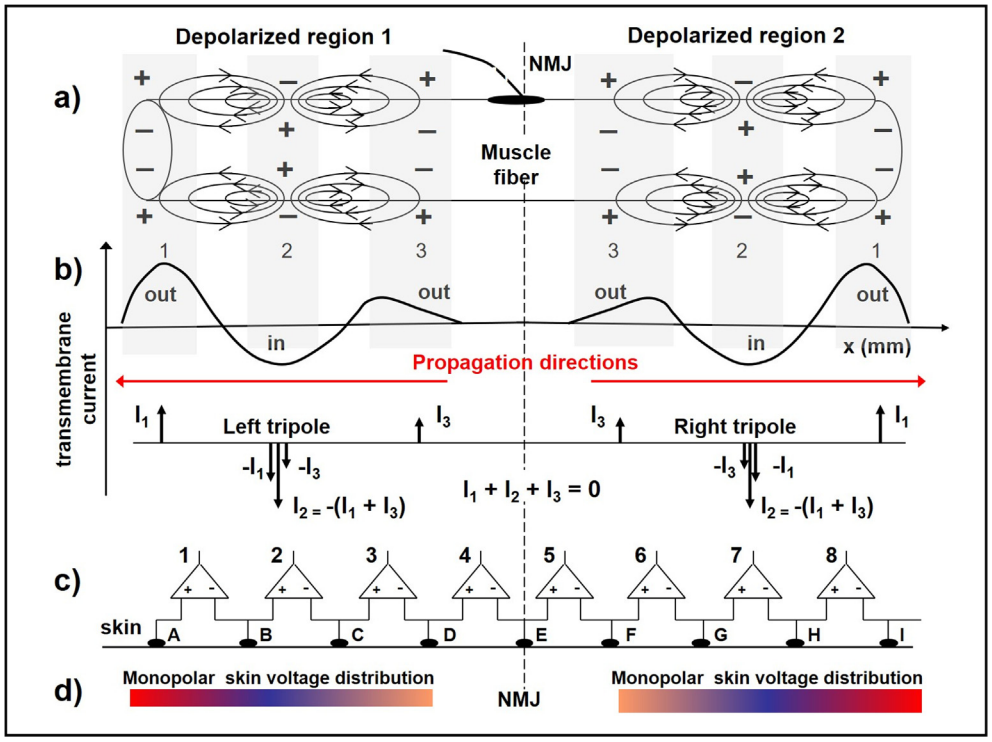

Fig. 2. Single fibers transmembrane currents. (a) Currents flowing across the membrane of a muscle fiber in the depolarized regions. The + and − signs indicate the local polarity of the membrane voltage and the grey bands indicate regions where current is going in or out. (b) Profile of the current in the inward (in, region 2) and outward (out, regions 1 and 3) directions across the fiber membrane and its approximate representation as a tripole. (c) Array of electrodes (A-I) and of differential amplifiers (outputs 1–8) detecting the propagating waveforms on the skin surface. (d) Color coded monopolar voltage distributions on the skin surface under the electrodes (red = positive, blue = negative) (Merletti et al., 1999a; Rosenfalck, 1969). Modified from www.robertomerletti.it. (For interpretation of the references to color in this figure legend, the reader is referred to the web version of this article.)

term "feature" is used in this work to indicate a property (such as amplitude or spectrum) that may change in time or from signal to signal. It is different from a "parameter" that is defined here as a fixed value associated to a model or to the system's anatomy (e.g. thickness of the subcutaneous tissue or electrode size).

2.2. The sources of the surface electrical potentials

2.2.1. Propagating sEMG components

The model presented in Fig. 2a describes the transmembrane current distributions associated to two APs (depolarized regions) propagating from the NMJ to the right and to the left in a single muscle fiber. These two APs reach the right and left muscle-tendon junctions where they extinguish, as described in Fig. 3. The transmembrane current profile is depicted in Fig. 2b. An approximated representation of this profile is provided by two current dipoles ($\pm I_1$ and $\pm I_3$, where $\pm I_1$ indicates the dipole $+I_1$ and $-I_1$, same for $\pm I_3$) forming the tripole $+I_1$, $-I_2$, $+I_3$ (where $I_2 = I_1 + I_3$). The first dipole represents the depolarization front and the second the repolarization tail of the AP. One tripole travels to the left and a mirror-like tripole travels to the right, in space, as a function of time, like cars moving in opposite directions in a street (Rosenfalck, 1969). The electric potential differences present across the membrane (Fig. 2a), indicated with + and −, not only produce the indicated currents but also an electric field (tripole field) in the surrounding volume, all the way to the surface producing the voltage distribution depicted in Fig. 2d, detected by the electrodes A-I.

Consider the linear electrode array depicted in Fig. 2c and a set of differential amplifiers associated to it. A differential amplifier provides an output voltage V_{out} proportional to the difference $V_+ - V_-$ between the inputs + and −. If V_+ increases V_{out} increases, if V_- increases V_{out} decreases. The colored bars (red = positive, blue = negative) depicted in Fig. 2d represent the surface "monopolar" potential distribution (voltage with respect to the reference electrode) on the skin, along a line under the electrode array, generated by the travelling tripoles. The positive wave-front propagating to the right encounters the non-inverting (+) input of each amplifier and then the inverting input (−) generating an upward swing followed by a downward swing of the amplifier's output voltage. The positive wave-front propagating to the left encounters the inverting input of each amplifier and then the non-inverting input generating a downward swing followed by an upward swing of the amplifier's output voltage. As a consequence, the time courses of the voltages of outputs 4 and 5 are mirror-like and so are the outputs 3 and 6 and the outputs 2 and 7, as well as 1 and 8 (see Fig. 4b). This explains (a) the symmetry of the propagating components of the waveforms reported in Fig. 4b and (b) the reason why the differential voltage between any two electrodes that are symmetric with respect to the NMJ (e.g. D-F, C-G, B-H, A-I) is theoretically zero and practically is mostly background noise, for this muscle configuration (fibers parallel to the skin and to the electrode array).

Not all the fibers belonging to a MU have their NMJ in the same location. The NMJs are often grouped in the middle of the MU in a region defined as the "innervation zone" (IZ) of the MU. In addition, the fiber-tendon junctions are scattered at the two ends of the muscle.

2.2.2. Non-propagating sEMG components

Non-propagating sources, and the related sEMG potentials, are mainly due to the generation (at the NMJ) and the extinction of the tripoles (at the end of each fiber). This phenomenon is depicted in Fig. 3a that describes how the tripole extinction, at one end of a single fiber, is usually modelled. At time t_1 the current tripole reaches the end of the fiber and its first current pole stops. At time t_2, dipole made by $+I_1$ and $-I_1$ ($\pm I_1$) is narrower (the distance between the two poles is reducing) and at time t_3 it has disappeared leaving only dipole $\pm I_3$. At time t_4 dipole I_3 is narrower and at time t_5 it has cancelled out. The two dipoles forming the tripole have opposite polarity; the electric field of dipole $\pm I_3$ partially cancels out the electric field of dipole $\pm I_1$ causing a rapid decay of the total field versus distance from the source. When dipole $\pm I_1$ disappears, the electric field of the residual dipole $\pm I_3$ decays more slowly versus distance from the source and contributes in a more uniform way to all nearby electrodes, (producing a voltage having rather similar contributions to the surface EMG channels), as indicated in Fig. 3c. This sequence of events is referred to as the "end-of-fiber" effect (see Section 2.4).

In the case of a MU, the amplitude of this end-of-fiber voltage is

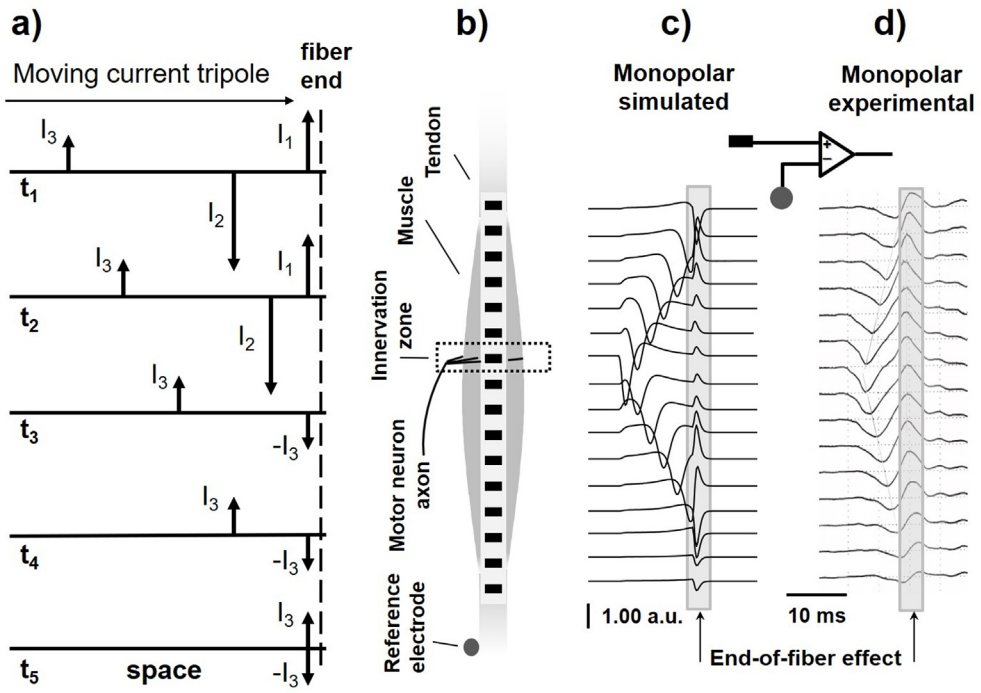

Fig. 3. The end-of-fiber effect. (a) Model of the extinction of a current tripole at the end of a single muscle fiber. As the propagating tripole reaches the fiber end, the poles stop, progressively overlap, and cancel out (see text for details). (b) Simulated MU whose fibers are all innervated and terminate at the same locations. The MU is parallel to the skin and to the electrode array, with center 6 mm below the skin. The MU has 200 fibers and its territory has a radius of 3 mm. The MU semi-length is 50 mm in the two directions. The skin and adipose layers have both 1 mm thickness. The IED is 10 mm. (c) Computer simulated monopolar signals detected by the linear electrode array indicated in b). The simulated muscle fiber conduction velocity value is 4 m/s. (d) Experimental monopolar MUAP detected over a healthy biceps brachii muscle with the same array indicated in b). The array does not reach beyond the fiber-tendon junctions. The depolarized zones, the spread of the NMJs, and the spread of the fiber-tendon junctions are likely wider than those simulated in c). Other differences may be due to the fiber conduction velocity, the volume conductor properties, the tripole approximations and the simulated point-like electrodes versus 1 mm thick, 5 mm long experimental bar electrodes.

inversely related to the spread of the fiber-tendon junctions (TS). As indicated in Fig. 4, its contribution to the differential signals is smaller than the contribution to the monopolar signal because of the largely common non-propagating components of this signal.

2.3. Propagating and non-propagating signals

If a linear array of N equally spaced electrodes is placed over a muscle and aligned with the fiber direction, N monopolar signals can be detected with respect to a reference electrode. N-1 SD (or bipolar) signals can be obtained, from adjacent electrodes, as indicated in Figs. 2c, 4b and 5b. N-2 DD signals can be obtained as indicated in Figs. 4c and 5c. The example applies to a muscle with fibers parallel to the skin. The case of pinnate muscles is more complex and not discussed in this tutorial. A detection modality or "electrode montage" (i.e. monopolar, SD, DD) strongly influences the shape of a MUAP and therefore the spectral features of the interference signal which is the algebraic sum of the MUAP trains.

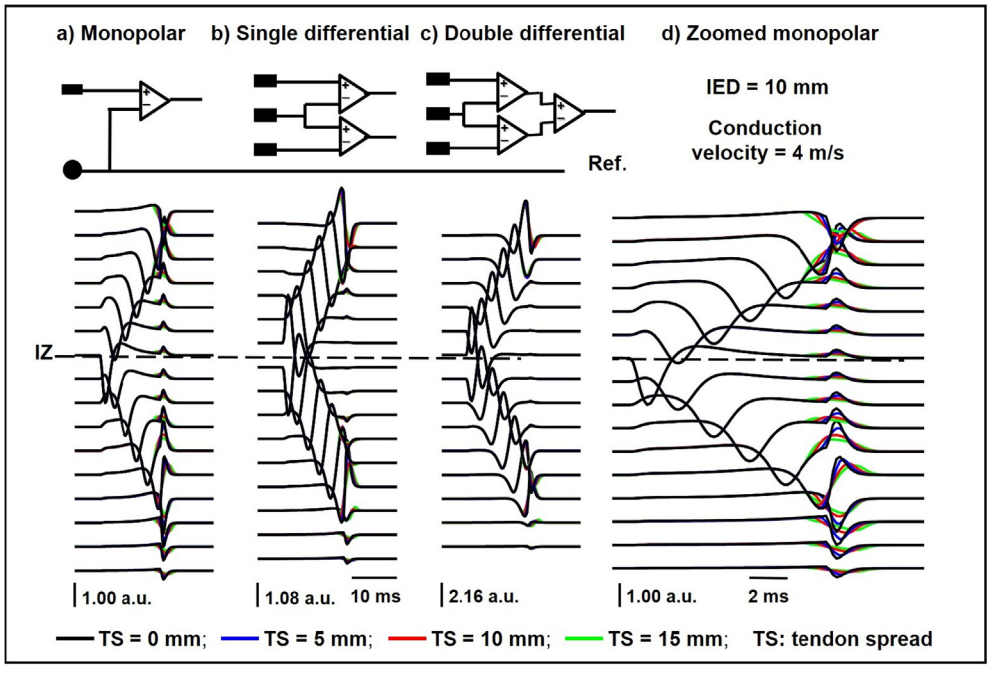

Fig. 4. Simulated action potential of a superficial motor unit as detected with a linear electrode array. All parameters of the model are the same as for Fig. 3 except for the spread of the fiber-tendon junctions (TS). Example of simulated (a) monopolar, (b) single differential (SD) and (c) double differential (DD) MUAP showing the different impact of the end-of-fiber effect, (d) time-zoomed version of the monopolar signal showing the effect of the spread of the fiber-tendon terminations. The simulated conduction velocity is 4 m/s and the spread of the NMJs is zero. The fiber-tendon junctions have a spread indicated by the different colors. The spread of the NMJs has a very similar effect. The thickness of the skin is 1 mm and adipose layers is 1 mm. The MU has radius 3 mm, with center at a depth of 4 mm in the muscle (6 mm under the skin) and is constituted by 200 fibers parallel to the skin. The MU semi-length is 50 mm in the two directions. Note the different amplitude scales: SD and DD signal amplitudes depend on the inter-electrode distance. The simulated electrodes are point-like. The a.u. units are arbitrary units that allow amplitude comparisons ; note the different scales.

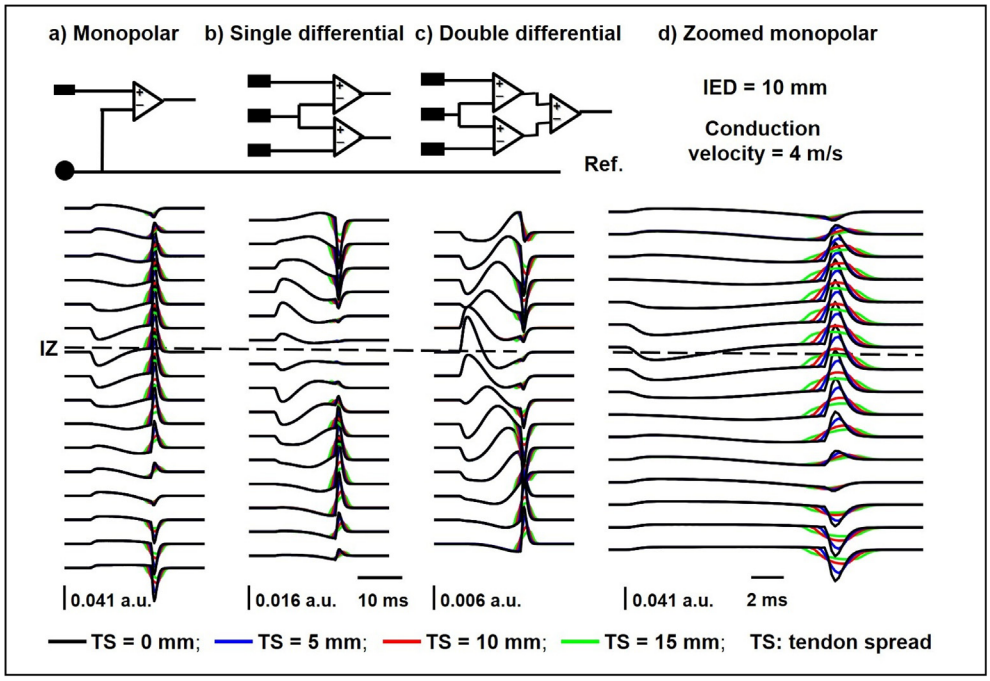

Fig. 5. Simulated action potential for a motor unit 22 mm below the skin as detected with a linear array. Except for the MU depth, all simulation parameters are the same as in Fig. 4. Example of a simulated (a) monopolar, (b) single differential (SD) and (c) double differential (DD) MUAP showing the different impact of the end-of-fiber effect, (d) time-zoomed version of the monopolar signal showing the effect of the spread of the fiber-tendon terminations. The fiber-tendon junctions have a spread (TS) indicated by the different colors. The value of the arbitrary unit of amplitude is the same as in Fig. 4. The peak-to-peak background noise value is about 0.01 a.u. (not indicated in the Figure). The SD and DD signals are near or below the noise level and therefore are barely detectable. The simulated electrodes are point-like. The a.u. units are arbitrary units that allow amplitude comparisons with respect to Fig. 4; note the different scales.

Fig. 4 depicts the three main detection modalities obtained from the simulation of a MU and a linear array of electrodes. The first modality (Figs. 4a and 3c), provides the voltage of each electrode of the array with respect to a reference and is referred to as the monopolar multichannel MUAP. The second (Fig. 4b), provides the output of the set of differential amplifiers depicted in Fig. 2c and is obtained by taking the difference between adjacent channels (usually along the fiber direction); it is referred to as the bipolar or SD montage. The third modality (Fig. 4c) provides the difference between adjacent SD channels, that is the double differential (DD) array of signals. Each of these signals defines a MU "signature" or "fingerprint" that repeats at each MU discharge. Fig. 4d is a zoomed version of Fig. 4a and shows the simulated effect of the spread of the fiber-tendon junctions (TS).

These three detection modalities are three "spatial filters" and provide three sets of signals that have different properties. The monopolar montage detects the entire information contained in the signal but is the most sensitive to common disturbances affecting all channels, to power line interference and to the end-of-fiber effect. The SD montage reduces these common components, facilitates the identification of the innervation zone (due to the characteristic " < " shape) and reduces the end-of-fiber effect: this may or may not be desirable depending on the application. The DD montage further attenuates non-propagating signals and, for this reason, is often chosen for estimating the propagation velocity of the MUAPs whose estimate is affected by the presence of non-propagating signals. At least two DD signals are required for this purpose. The four electrodes needed to obtain the two DD signals should cover a portion of the MU with unidirectional propagation of the action potentials (on the same side with respect to the innervation zone). This requires relatively long muscles or a small inter-electrode distance (IED). In addition, the three detection modalities have different detection volumes and therefore detect a different number of MUs, that is the monopolar montage can detect "far" sources while the SD and DD modalities are more selective and detect "near" sources. Different lengths of the depolarized regions and different spreads, in space, of the fiber-tendon junctions of a MU imply different widths and amplitudes of the end-of-fiber effect, as indicated by the colored curves in Figs. 4d and 5d.

For progressively deeper MUs both the propagating and non-propagating components of the MUAP decrease in amplitude, but at different rates. The first decreases faster, as mentioned above; consequently, the two components become more comparable, as indicated in Fig. 5 for a MU identical to that simulated in Figs. 3 and 4 but placed at 22 mm below the skin. In this condition (a) the signal amplitudes are near the background noise level (about 0.01 a.u.) and (b) the propagating and non-propagating components have similar amplitudes. Non-propagating MUAPs, presumably from deep or lateral MUs, are frequently observed in experimental situations.

2.4. Detection volume and the issue of crosstalk

The current distribution in the space surrounding a muscle fiber (Fig. 2a) generates the potential distribution on the skin surface. As the vertical (or lateral) distance between the detection system and the source increases, the potential on the surface decreases. In particular, the propagating components decrease faster than the non-propagating end-of-fiber effect so that, at some distance the second dominates over the first (Fig. 5). The largest experimentally detected monopolar MUAPs have peak-to-peak amplitude of 1–2 mV while the background noise has peak-to-peak amplitude of about 1% of this value. The end-of-fiber effect may reach the noise value a few cm away from the MU generating it. Therefore, propagating and (mostly) non-propagating signal components generated by a MU can be detected by electrodes placed on regions nearby the muscle of interest, as shown in Fig. 6 and in (De Luca and Merletti, 1988; Farina et al., 2002b; De Luca et al., 2012), possibly on other muscles. The computer simulations reported in Fig. 5 predict that, for IED = 10 mm, the contribution of the simulated superficial MU producing the largest detectable MUAP can still be barely detected if *the same* MU is moved at a depth of 22 mm below the skin. These considerations bring up the concepts of detection volume and crosstalk. Given a detection system (single electrode pair, 1D or 2D electrode array, monopolar, SD, DD, other spatial filters), how far from such detection system can a source (a simulated tripole, a muscle fiber, a MU) be and still contribute a signal above the noise level? The locus of these distances in space defines the detection volume. Alternatively, given a fixed source, how far from it, on the skin, could a second detection system be and still detect a contribution above the noise level? The second detection system could be on a second muscle and detect "some" signal generated by the first. The signal detected on a muscle but generated by another one (that could be below or beside it) is referred to as "crosstalk". Figs. 6–8 illustrate this phenomenon. In

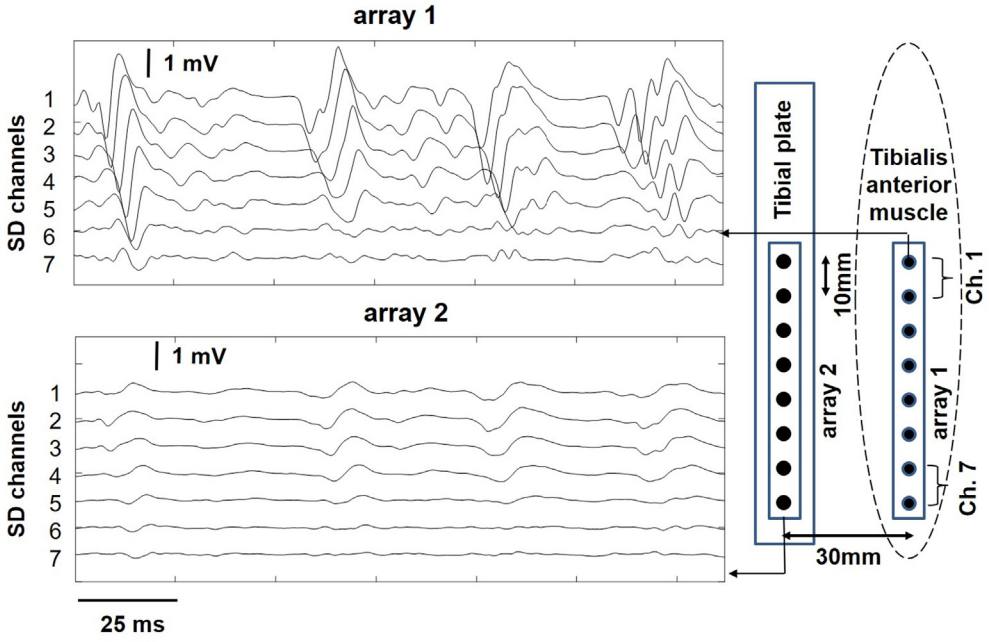

Fig. 6. Examples of experimental SD signals detected on the tibialis anterior and tibial plate, during a slight contraction of the tibialis, by two electrode arrays having IED = 10 mm. Array 1 is on the muscle and array 2 is 30 mm medially. The end-of-fiber components, evident in array 2, are larger than those predicted by the model used to create the synthetic signals depicted in Fig. 4 and Fig. 5, likely because of the presence of bone. (Courtesy of V. Devecchi).

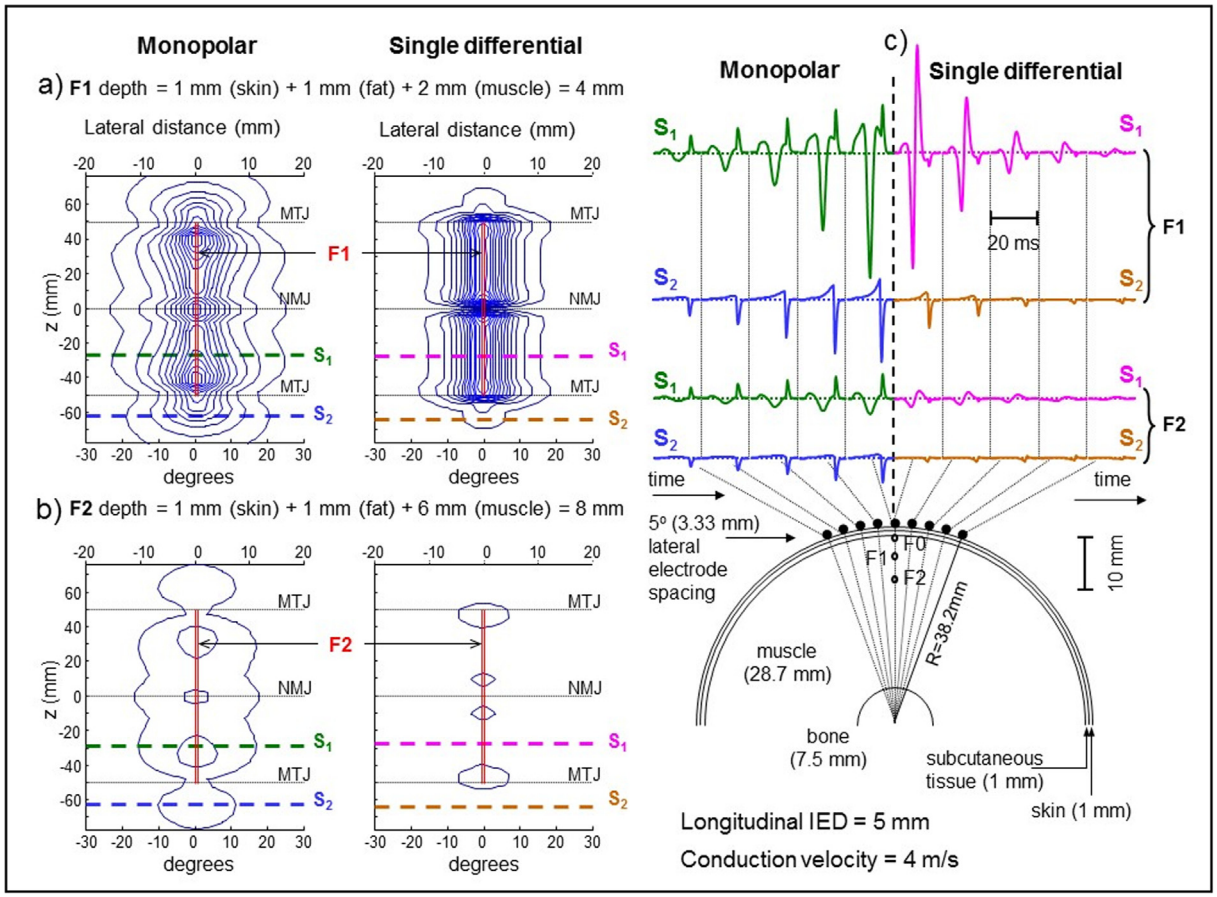

Fig. 7. Computer simulations, with a cylindrical model, of the decay in space of the surface AP generated by two fibers at 4 mm (F1) and 8 mm (F2) below the skin. See text for explanation. (a) Monopolar and SD iso-peak-to-peak amplitude contour plots of fiber F1 normalized with the respect to the SD V_{ppmax} produced by the most superficial fiber F0. The most external contour corresponds to the detectability level (1% of V_{ppmax}). Contour levels are separated by 1% of V_{ppmax} (b) Same as in a) for a fiber (F2) placed 8 mm below the skin. (c) Decay in space (on the skin surface) of the monopolar and SD AP generated by a fiber at 4 mm below the skin (F1) and one at 8 mm below the skin (F2). The most lateral SD potentials are below or at the noise level (see text for explanation). The colored dashed lines indicate the sections S1 and S2 corresponding to the signals depicted in c). NMJ = neuromuscular junction, MTJ = fiber-tendon junctions. Model parameters: $\sigma_{bone} = 0.02$, $\sigma_{fat} = 0.05$, $\sigma_{skin} = 1$, $\sigma_{muscle\_r} = 0.1$, $\sigma_{muscle\_z} = 0.5$ $(\Omega m)^{-1}$; lateral IED = 3.33 mm (5°); longitudinal IED = 5 mm; point-like electrodes.

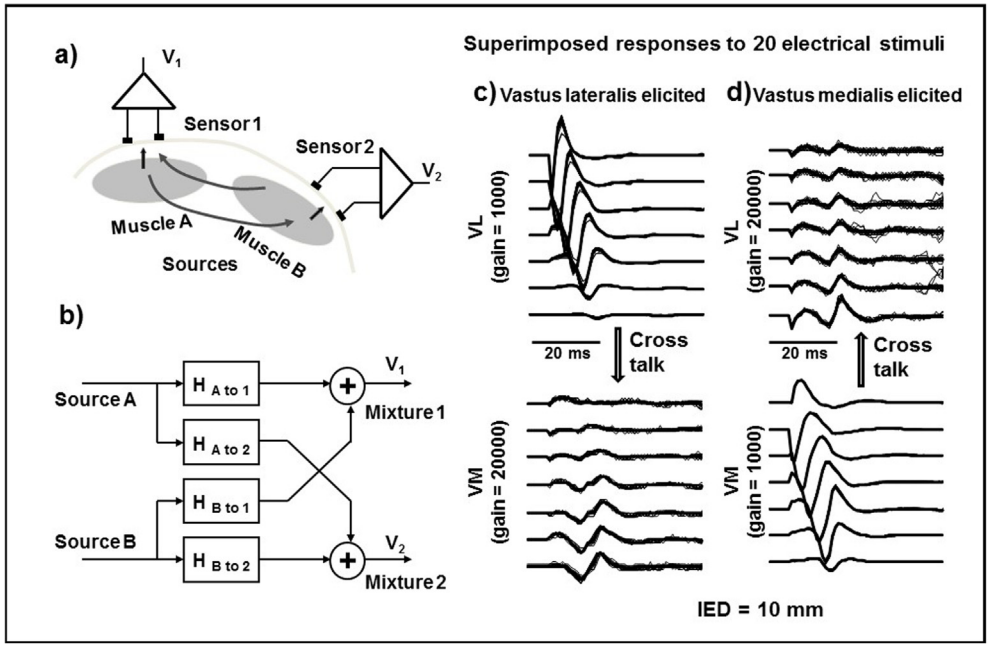

Fig. 8. Crosstalk between muscles. (a) The concept of crosstalk, (b) schematic model of crosstalk, (c) sEMG signals detected on the vastus medialis (VM) during electrical stimulation of the vastus lateralis (VL), (d) sEMG signals detected on the vastus lateralis (VL) during electrical stimulation of the vastus medialis (VM). Note the different amplifier gains and the larger crosstalk signal at the muscle-tendon region. Both electrode arrays are between the innervation zone and the muscle-tendon junction of the respective muscles. The circumferential distance between the arrays is 39 mm. $H_{A\ to\ 1}$ is the "transfer function" (that is the filter) from the source A signal to the mixture 1 signal. Fig. 8c and d are from Fig. 1 pg 685 of (Farina et al., 2002b), with permission.

addition, the detection volume is strongly affected by the IED (De Luca et al., 2012; Vieira et al., 2017) as well as by a number of other parameters (e.g. tissue conductivities) as indicated by (Farina et al., 2002b; Roeleveld et al., 1997).

Fig. 6 depicts experimental differential sEMG signals detected on the tibialis anterior muscle and on the tibial plate, with two arrays placed 30 mm apart, during a slight contraction of the tibialis. Mostly propagating MUAPs are detected by array 1 (on the muscle) and mostly non-propagating signals are detected by array 2 placed 30 mm medially at the tibial plate. Some of the non-propagating signals detected by array 2 appear to be generated under array 1 (they are synchronized with them) and are larger than those a model would predict for 30 mm distance (Fig. 5b shows signals at the noise level at distances of 22 mm) likely because of the presence of the tibia bone distorting the field. The model parameters should be adjusted for each individual to match the collected signals, a problem that exceeds the purpose of this tutorial but justifies the use of models as investigational tools.

Crosstalk is the signal detected over a muscle but generated by other muscles below or beside it (De Luca et al., 2012; De Luca and Merletti, 1988; Vieira et al., 2017) as shown in Fig. 8a. This signal is due to the lateral spread of each tripole field and to the end-of-fiber effect, as shown in Figs. 5–7. Consequently, in general, the sEMG is a mixture of signals due (a) mostly to sources just below the skin under the electrodes (smallest distance) and (b) to crosstalk generated by other muscles below or beside the muscle of interest. It is therefore of importance to be aware of the lateral spread of the potential generated by a source (tripole) moving along a fiber and extinguishing at the end of it. For this purpose, let us consider a superficial source (at the boundary between a thin subcutaneous fat-skin layer and the muscle). This source would generate the largest possible potential on the skin, that is taken as a reference. Experimentally, such a source would be a MU whose MUAP is observed to have a peak to peak value (V_{ppmax}) of 1–2 mV (depending on the number of fibers) as indicated in Fig. 6. The peak to peak value of the background noise is in the range 0.01–0.02 mV, that is 1% of V_{ppmax}, as indicated above. This means that if the same source were placed at a depth d such that its surface potential had $V_{pp} = 0.01V_{ppmax}$ it would be barely detectable from noise. The depth d would then be the maximal depth at which that source would still be detectable, that is at the edge of the detection volume. This condition has been modeled with a cylindrical model simulating the APs of three fibers, F0, F1 and F2, using the model developed by (Farina et al., 2004). Results are reported in Fig. 7 where surface signal intensities are represented as "contour plots" spaced by 1% of the largest (V_{ppmax}) signal which is generated by fiber F0 just under the fascia and taken as reference. A "iso-V_{pp} contour plot" is the locus of points on the surface where the signal has the same peak-to-peak value.

Fig. 7a shows the iso-V_{pp} contour plots of the simulated monopolar and SD surface signal generated by the fiber F1, placed below 1 mm of skin, 1 mm of subcutaneous tissue and 2 mm of muscle tissue. The contour plots are spaced by $0.01V_{ppmax}$ and the most external contour is at $0.01V_{ppmax}$, that is the locus of the points where the peak to peak value is at the noise level and no longer detectable. That is the spatial extent of crosstalk. The simulation is repeated with the same fiber at a depth such that the surface monopolar or SD V_{pp} is near the noise level (F2), that is at the edge of the detection volume (Fig. 7b). Fig. 7a and b show the contour plots for the monopolar and SD signals during the generation, propagation and extinction of the APs. Fig. 7c shows the monopolar and SD signals (APs) detected on the surface of the cylinder at section S_1 and S_2 indicated in Fig. 7a and b. The SD signal reaches the noise level when the fiber (F2) is at about 8 mm below the skin (Fig. 7b). The monopolar and the SD surface potentials can barely be detected at 15–20° angle, that is 10–13 mm lateral distance, and at 10° angle, that is 6.6 mm lateral distance, respectively, from the point above the fiber. This indicates a fast decay of EMG amplitude with distance, as indicated in Fig. 7c for the two fibers F1 and F2. This approach provides a model-based indication of the maximal detection depth and of the maximal lateral potential spread for a source moving along a line parallel to the skin.

A way to experimentally assess crosstalk is to electrically stimulate one muscle on its motor point and detect signals from nearby muscles, that are presumably inactive as indicated by the lack of propagating potentials in their sEMG (De Luca and Merletti, 1988). Fig. 8c and d show experimental SD signals detected by an electrode array placed on the distal portion of the vastus lateralis (VL) and a second array placed on the distal portion the vastus medialis (VM) when either muscle is electrically stimulated at its motor point with 2 pulses/s for 10 s.

The two arrays are about 39 mm apart. Twenty responses are superimposed to show repeatability. Note that the signal detected on the non-stimulated muscles is amplified 20 times more than the one on the stimulated muscle and is near the noise level (Farina et al., 2002b). The crosstalk signal is a "filtered" version of the source signal (generated by the stimulated muscle). The operation performed on the source signal to

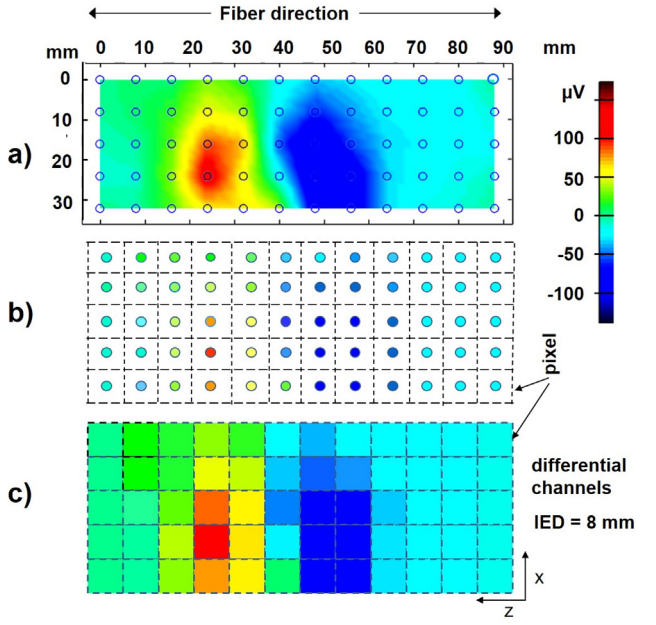

Fig. 9. Sampling sEMG images in space. (a) Instantaneous analog spatial distribution of a SD MUAP voltage, propagating along z, sampled by a grid of 5 × 13 electrodes, applied on a biceps brachii, generating 5 × 12 SD channels, (b) voltage detected by each electrode pair (channel) in the fiber direction, (c) for cosmetic reasons, the instantaneous voltage detected by each channel is usually associated with the corresponding pixel of the image. Circular electrodes have 3 mm diameter. Consider the length of this MUAP (about 60 mm) and its width (about 50 mm) in space. A similar MU placed about 50 mm lateral (in the x direction), with respect to the centerline of the array, would provide crosstalk on some of the channels. Such MU might or might not belong to the same muscle. Assuming a muscle fiber conduction velocity of 4 m/s the time duration of the MUAP detected by each channel along z would be about 15 ms.

generate the crosstalk signal is the "transfer function" of the filter.

Another approach, investigated by (Vieira et al., 2017), implies to detect the MUAP of one MU in one muscle with intramuscular wires and the synchronized sEMG contribution of that MU on a nearby muscle. While the comparison of the approaches is left to the interested reader, this work underlines how crosstalk strongly increases with increasing the IED used in the SD detection.

3. The concept of sampling an image in space and in time

3.1. Sampling in space

The concept of spatial sampling, described in Fig. 1a, is further explained in Fig. 9. Fig. 9a depicts an instantaneous SD analog voltage distribution sampled (in space) by a grid of 5 × 13 electrodes, 8 mm apart in each direction, providing 5 × 12 SD detection points. Voltage values in each point are represented by colors as indicated in the color scale. Fig. 9b shows the SD detection array; the circle representing each electrode pair is filled with a color representing the average (in space) voltage under its area at the specific time of this frame. This is the information actually obtained from the spatial sampling process. The "color" of an electrode is usually attributed to the entire pixel the electrode belongs to. This representation is purely cosmetic and not rigorously correct (Fig. 9c). What is actually available is the spatial mean of the voltage under each electrode. This representation raises a number of questions each of which is addressed subsequently (Figs. 11–14). What is the effect of electrode size? How close should the electrodes be to allow reconstruction (by interpolation) of the analog image in Fig. 9a starting from the sampled image of Fig. 9b? When is such reconstruction clinically important?

3.2. Effect of electrode size: The transfer function of a single electrode

The concepts of sampling in space (by a 1D or a 2D electrode array) and in time (by an electronic sampler) are depicted in Fig. 10a and b. The physical size of the metal or conductive gel electrode implies the averaging of the voltage distribution under the electrode area, as indicated in the 1D example depicted in Fig. 10c. In turn this implies a low-pass filtering operation in space and therefore a loss of details (Afsharipour et al., 2019; Cattarello et al., 2017; Dimitrova et al., 1999; Farina and Merletti, 2001a,b; Fuglevand et al., 1992; Helal and Bouissou, 1992).

A filter operates on an input signal and generates an output signal by attenuating or enhancing certain harmonics (frequency components) of the first. Such a device can operate on signals in space or in time and the "operator" is called the "transfer function of the filter" or simply "transfer function". For example, a filter applied to an audio signal can attenuate the high or the low pitch sounds. The spatial transfer function operates on the spatial Fourier transform of the signal. The frequency axis of these spatial transfer function and spatial Fourier transform are expressed in cycles/meter (cycles/m or c/m). The transfer function of the averaging filter introduced by an electrode is depicted in Fig. 11 for four diameters of circular electrodes. A diameter of 1 mm implies almost no filtering of the sEMG but a diameter of 5 mm implies a 3 dB point (half power) at 100 c/m and a 10 mm diameter implies a low-pass filtering effect with a 3 dB point at 50 c/m and consequent loss of detail and reduction of RMS estimate, as shown in Fig. 12.

3.3. Differential signals and the effect of inter-electrode distance

Biosignal amplifiers have a differential gain and an undesired common-mode gain. The first, usually large (e.g. A_d = 500–2000), applies to the differential signal whereas the second, usually very small (e.g. A_{cm} = 0.1), applies to the voltage common to both inputs (average). For example, consider two instantaneous inputs of 99 mV and 101 mV (that is 100 mV common-mode and 2 mV differential). If A_d = 1000 and A_{cm} = 0.1, the output voltage will be $1000 \cdot 2\,mV + 0.1 \cdot 100\,mV = 2010\,mV$. This will be discussed in greater depth in another tutorial. Differential detection of sEMG signals is preferred to monopolar detection when attenuation of common-mode signals and of non-propagating signal components, or identification of innervation zones, are desirable (see Figs. 1a, c and 4b).

Differential detection can be obtained in two ways:

(1) Using differential front-end amplifiers. In this way, common-mode signals will be strongly attenuated by the differential amplifier and monopolar signals will not be available for subsequent processing (that is occasionally of interest).
(2) Acquiring monopolar signals and computing differential signals by software. The availability of monopolar signals will allow the subsequent application of spatial filters since the entire information contained in the signals will be available, including the common-mode signals.

In the first case a high common mode rejection ratio (CMRR) is required. This ratio is defined as A_d/A_{cm} and is often expressed in dB as $20Log_{10}$ (A_d/A_{cm}). Acceptable values are near 100 dB ($A_d/A_{cm} = 10^5$). In the second case the monopolar front-end amplifiers must have identical gains and frequency behaviors (magnitude and phase) so that the difference between the outputs will be computed between equally scaled signals and the common-mode signals (present on all channels with equal amplitude) will be cancelled. This condition is technically difficult to achieve. Other considerations (e.g. concerning input impedance) apply to both detection techniques. The first technique will be discussed in the following paragraphs (Afsharipour et al., 2015; Lindstrom and Magnusson, 1977; Lynn et al., 1978).

Consider the differential amplifier depicted in Fig. 13a. Its output is

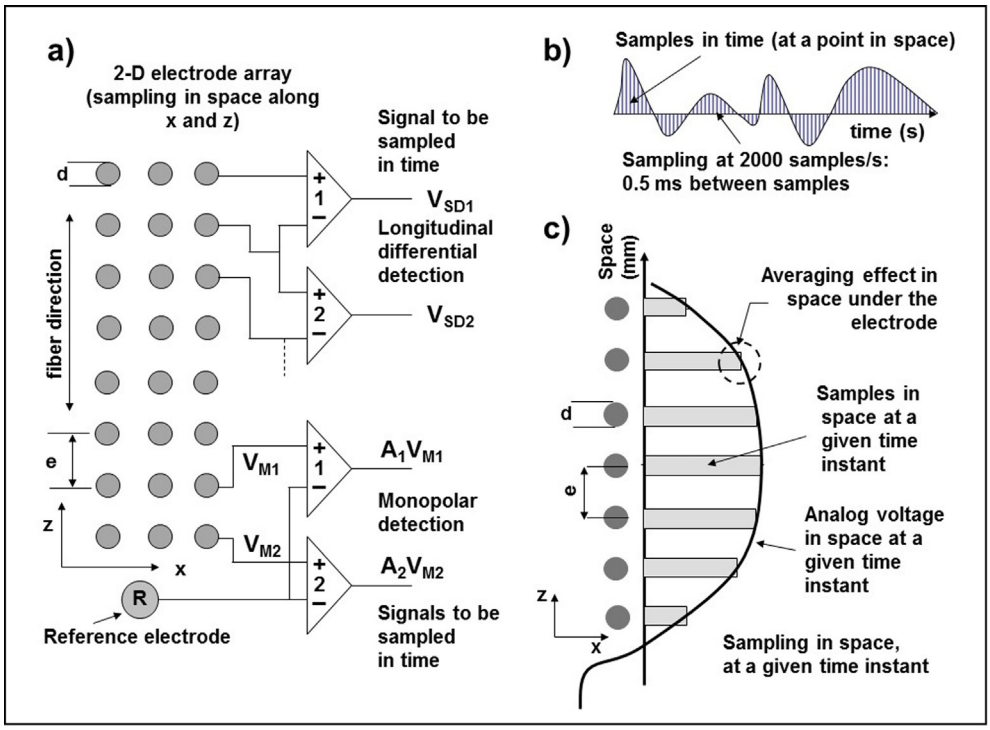

Fig. 10. (a) Portion of an electrode grid with example of differential (top) and monopolar (bottom) detection. Differential detection can be along the columns or along the rows or diagonally. Monopolar detection is with respect to the reference electrode R placed on an electrically inactive area of the skin. Either rows or columns are usually aligned with the fiber direction (columns in this example). See text for further comments. (b) Example of sampling a signal in time. (c) Example of sampling a signal in space by means of circular electrodes. The detected voltage is the average of the 2D voltage distribution present under the electrode (represented in 1D in the figure). This averaging implies the low-pass spatial filtering operation described in Figs. 11 and 12.

proportional to the difference between the voltages present in points A and B, which are two spatial samples, separated by the IED *e*, along *x*, expressed in meters. Consider then four spatial harmonics of the signal propagating along x and having the same amplitude and the four wavelengths $\lambda_1 = 4e$, $\lambda_2 = 2e$, $\lambda_3 = 4e/3$ and $\lambda_4 = e$ corresponding to spatial frequencies $f_1 = 1/(4e)$, $f_2 = 2/(4e)$, $f_3 = 3/(4e)$ and $f_4 = 4/(4e)$, expressed in c/m (Fig. 13b). As they propagate under A and B they generate four different sinusoids in time, at the output C, whose amplitudes are depicted in Fig. 13c. The system behaves differently for different input frequencies and is therefore a filter. For $\lambda \gg e$ (left portion of the plot in Fig. 13c) the filter approximates a spatial differentiator, which is its desired performance. The propagating spatial distribution of the sEMG potential has many harmonics that are amplified with different gains by the differential system depicted in Fig. 13a. The plot of the "filter gain" in Fig. 13c describes how such gain depends on the wavelength λ (or the spatial frequency $f_s = 1/\lambda$) of the harmonics.

The combined effects of the filter due to electrode size and the filter due to the IED are depicted in Fig. 14. The filtering in space has a counterpart in time for propagating signals (not for non-propagating signals). The wavelength λ of a spatial harmonic having frequency ($f_s = 1/\lambda$) and propagating under one of the monopolar detection electrodes in Fig. 1a takes the time T to pass under the electrode at the propagation velocity $u = \lambda/T$ generating a sinewave in time having frequency $f = 1/T$. It is therefore $u = \lambda/T = f/f_s$ or $f = u\, f_s$. Therefore, the signal in time detected by the monopolar electrode has the same shape of the signal in space with a frequency scaled by the proportionality factor *u,* which is the muscle fiber conduction velocity.

The same frequency scaling applies to the differential signals and to the transfer function of the spatial filters depicted in Fig. 14. Three frequency scales are indicated in Fig. 14 for values of the conduction velocity u of 3, 4 and 5 m/s, showing that the same spatial distribution of monopolar sEMG results in different time and frequency scaled sEMG (that is different filters in time) depending on the conduction velocity. In other words, the same spatial potential distribution moving under an electrode at a lower conduction velocity produces a wider waveform in time. As an example, the same car takes a longer time to pass in front of a camera if its speed is lower.

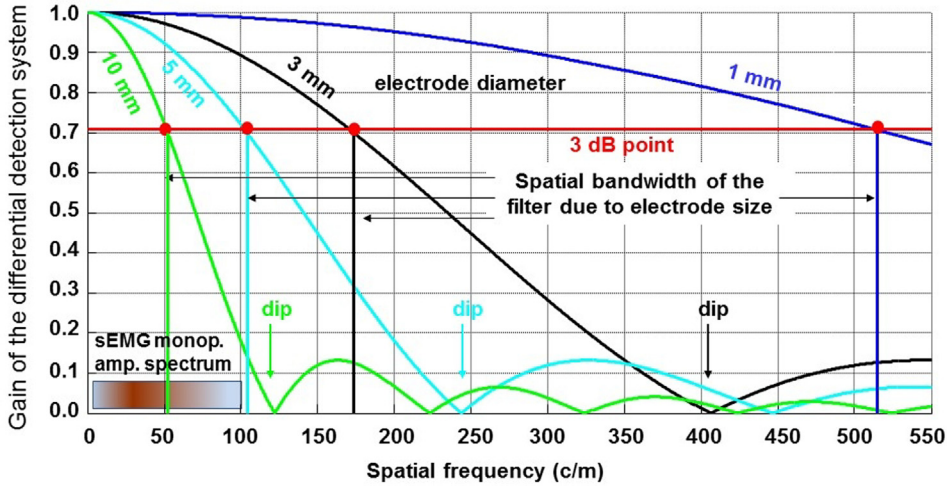

Fig. 11. Plots of the magnitude of the transfer functions (in the spatial frequency domain) of circular electrodes of four diameters: 1, 3, 5 and 10 mm. The spatial filter introduced by the electrode is a low-pass whose cut-off frequency (3 dB point) is indicated for each electrode diameter. Electrodes with diameter of 1 mm or 3 mm apply acceptable filtering, electrodes with diameter of 5 mm reduce the high frequency components of the sEMG, while electrodes with diameter of 10 mm or more markedly reduce the high frequency components of the sEMG and modify its shape (see also Fig. 12). The bar of the sEMG monopolar amplitude spectrum (Fourier transform of the sEMG signal) indicates larger harmonics with a darker color.

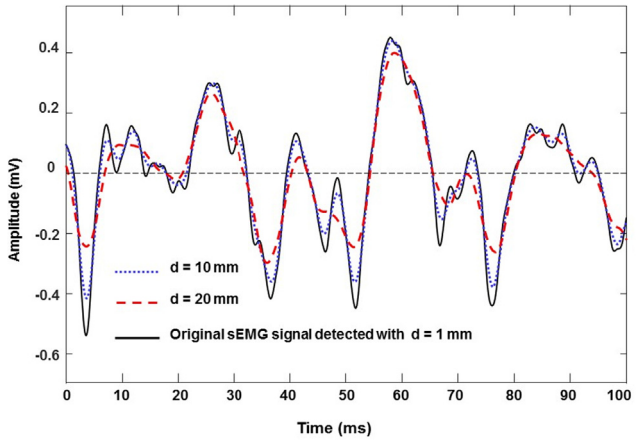

Fig. 12. Low-pass filtering effect for two different diameters of a circular electrode on a monopolar sEMG signal in time. The signal has been acquired with two pin electrodes having d = 1 mm and has been filtered with the transfer functions depicted in Fig. 11. Observe the strong attenuation of the sharp peaks due to electrode size.

Consider a differential detection system made of two electrodes having the rather common values d = 10 mm and IED = e = 20 mm (Fig. 14b). Consider also three MUs at the same depth but with conduction velocity of 3, 4 and 5 m/s respectively, generating three spatially identical signals propagating on the surface of the skin. Their respective signal contributions (MUAPs) and transfer functions will be the same in space but different in time because the three sources move at different velocities. The transfer function (in the f (Hz) domain) of the filters associated with the three MUs will have the first dip at 150 Hz, the second at 200 Hz and the third at 250 Hz, all in the middle of the respective sEMG bandwidths that are 300, 400 and 500 Hz, respectively.

The overall signal is the sum of the three (spatially identical) contributions of MU1, MU2 and MU3, which are differently filtered. The Fourier transform (magnitude spectrum) of the sum signal is the sum of the three Fourier transforms and the power spectrum of the total signal is the square of the magnitude spectrum (not the sum of the three power spectra). Since the dips of the spectra do not coincide, they are smoothed out by the sum and may not be so sharp in the overall spectrum. The waveshapes of the MUAPs of MU1, MU2, MU3 are substantially altered by this filtering. This may be more or less relevant, depending on the purpose of the measurement, and is discussed later in the example given in Fig. 16.

The differential detection system removes non-propagating signals, DC components in space, power line interference and other signals that are *identical* under both electrodes of a pair (common-mode signals). This is often not the case, in particular when the differential signals are obtained by software difference between amplified monopolar signals. For example, the differential signal obtained from the amplifiers associated to electrodes 1 and 2 in Fig. 10a is $V_{SD} = A_1V_{M1} - A_2V_{M2}$ and an artificial differential signal is created if $A_1 \neq A_2$, even if $V_{M1} = V_{M2}$, where A_1 and A_2 are the amplifications (in magnitude and phase) of the amplifiers associated with electrodes 1 and 2. A correct SD signal is obtained only if $A_1 = A_2$.

Anticipating a remark belonging to another tutorial, consider a compression of the monopolar sEMG amplitude spectrum, that is a shift to the left of the dark region of the bar indicated in Fig. 14a and b. The resulting change of mean or median spectral frequencies would be different for different values of d and IED (Farina et al., 2002b; Fuglevand et al., 1992; Griep et al., 1978).

The considerations provided above apply to a single electrode pair as well as to electrode pairs that are part of an array. They are important if the shape of the sEMG signal is important (e.g. when MUAP shapes should be compared or spectral changes of the interference pattern should be monitored). In order to limit the spatial filtering introduced by the IED and avoid spectral dips within the sEMG bandwidth (Figs. 14 and 16), the IED should be in the range of 5–10 mm. This small distance may create problems with gelled electrodes whose

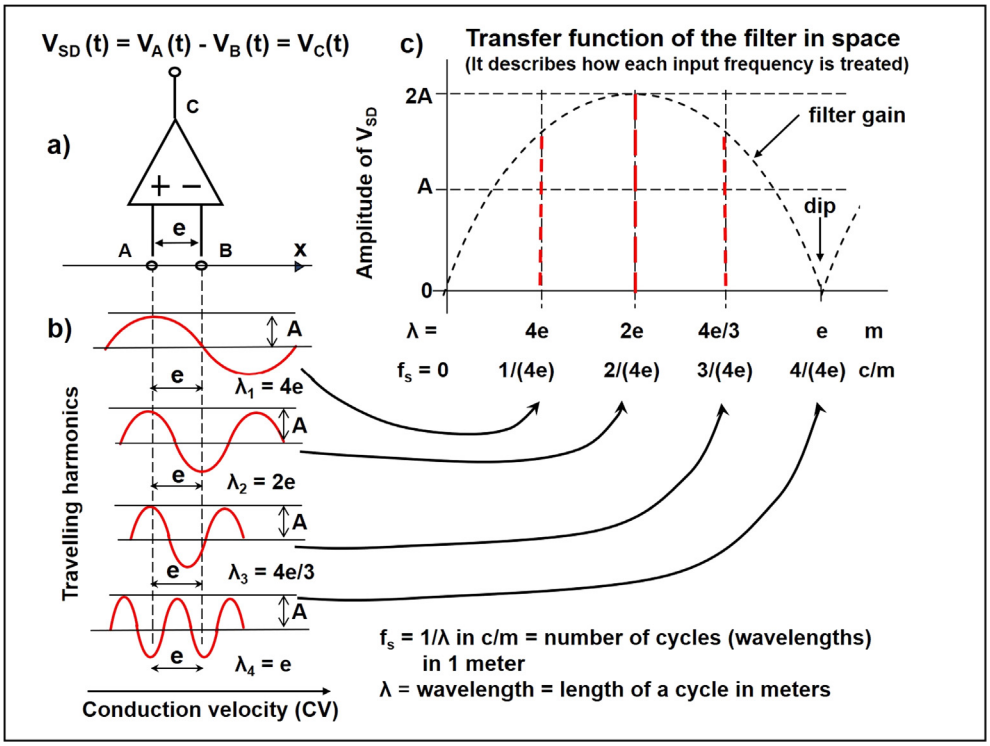

Fig. 13. Spatial filtering effect of a differential detection system. (a) Differential detection system, (b) four harmonics of the spatial signal distribution moving along x with velocity u. (c) Amplitudes of the four harmonics observed in point C (V_{SD}).

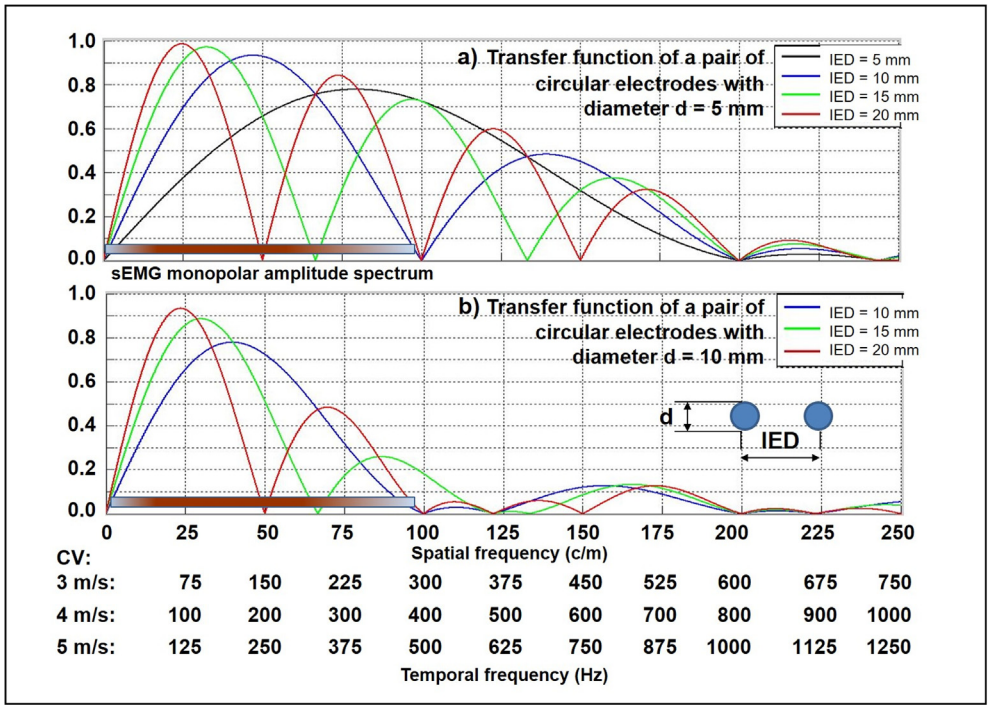

Fig. 14. Overall transfer function of a pair of circular electrodes. The transfer function is depicted for two diameters (5 mm and 10 mm in (a) and (b) respectively and three inter-electrode distances (10 mm, 15 mm and 20 mm). The sEMG monopolar amplitude spectrum bar (Fourier transform of the sEMG signal) shows larger harmonics with darker colors. The sEMG bandwidth and the transfer functions of the filters associated to the detection system in the f (Hz) domain are obtained by scaling f_s (c/m) by the conduction velocity factor u (m/s). Three examples are provided for conduction velocities u equal to 3, 4 and 5 m/s that correspond to the three indicated different scales of temporal frequency (see www.robertomerletti.it for more detailed explanations and examples).

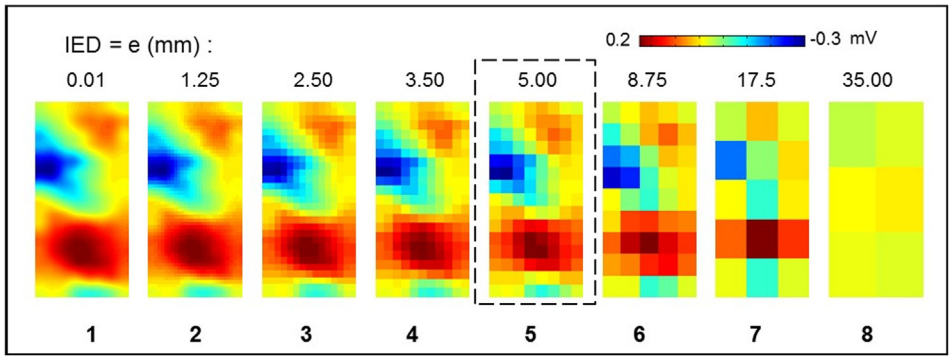

Fig. 15. sEMG image interpolation. Image 5 is the spatially sampled version (e = 5 mm, electrode diameter = 1 mm) of an analog sEMG frame from a biceps brachii muscle. Image 1 is the result of interpolation with a "sinc" function and can be considered as the reconstructed analog image. All the other images (2–8) are obtained by resampling image 1 in space. Images 1 to 4 can still be reconstructed by interpolation of image 6 but not from images 7 and 8. Image size: 35 × 70 mm. Courtesy of S. Soedirdjo.

gel may leak between two electrodes that then become one electrode. Particular care should then be used to avoid this problem and fluid gels should be avoided. Research should focus on the development of sEMG pre-gelled electrodes with semisolid gel that would not leak between electrodes, or on dry pin electrodes that would partially perforate the stratum corneum.

3.4. The transfer function of an electrode grid: Interpolation and truncation effects

As the High Density sEMG is acquiring clinical relevance, the issues related to the "sEMG imaging" technology are becoming more and more important. Sampling a 2D signal (image) in space is conceptually similar to sampling a 1D signal in either space or time (Fig. 9 and Fig. 10). As indicated by the Nyquist-Shannon theorem, all the signal information content can be recovered if sampling is performed at a frequency higher than twice the maximal frequency (highest harmonic) of the signal. Only in this case the original analog image (if relevant) can be faithfully reconstructed by proper interpolation and its features can be computed correctly. The highest spatial frequency of an instantaneous monopolar sEMG map (a frame of the movie), either in the x or z direction, is in the range of 70–90 cycles/m with occasional peaks above 100 cycles/m as reported in (Afsharipour et al., 2019; Merletti et al., 2013; Merletti and Farina, 2016). Although a study on many subjects and muscles is missing, the theoretical spatial sampling frequency should be above 200 samples/m, that is e < 1000/200 = 5 mm. However, the signal alterations (aliasing) introduced by spatial sampling at 100 samples/m, that is e = 10 mm, seem to be limited and acceptable for most purposes. They become more and more serious for e > 10 mm because of the introduction of dips into the bandwidth of the sEMG (Fig. 14). The clinical relevance of the introduced signal alteration depends on the purpose of the measurement. For example, it is not relevant if the purpose of the measurement is just to identify muscle activation intervals.

The following part of this section requires some basic knowledge of image analysis and processing. Fig. 15 shows a sEMG frame recorded with IED = e = 5 mm (image 5) with pin electrodes (d = 1 mm). Images 1–4 have been obtained by interpolation with a *sinc function* (optimal interpolation) while images 6, 7, 8 have been obtained by resampling image 1. Image 1 can still be recovered (with error of the spatial RMS acceptable for most applications) from image 6 but not from image 7 or 8. These considerations are important for advanced applications requiring image interpolation. Inter-electrode distances of 5–8 mm should be used when the entire information content of the image is needed, and values of 8–10 mm should be considered as a compromise for other applications and should not be exceeded. Values of IED above 10 mm can be accepted if the required information is just an indication of muscle activity and alterations of MUAP shapes can be

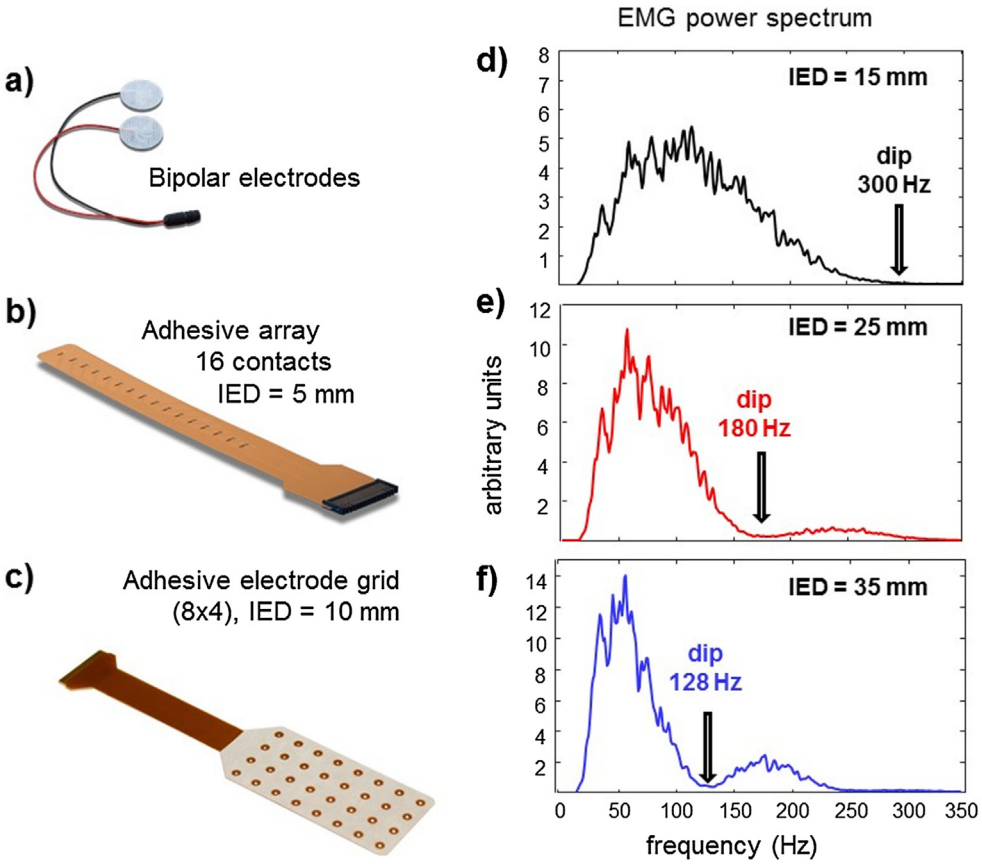

Fig. 16. Electrode types and presence of dips in experimental signals. (a) Example of electrode pair, (b) example of a 1D electrode array, (c) example of a 32 electrode grid; (d), (e), (f) power spectrum of three signals simultaneously obtained from a biceps brachii and from three pairs of electrodes, selected among the contacts of the linear array, centered around a central fixed point, with IED of 15 mm, 25 mm and 35 mm. The frequency of the three dips is compatible with a muscle fiber conduction velocity of 4.5 m/s. The dip for IED = 15 mm is not evident because the spectrum of the specific signal is narrow. It would be more evident for a spectrum reaching 400–450 Hz. The RMS value of each signal is the square root of the area under the corresponding spectrum and is therefore affected by IED (De Luca et al., 2012). Courtesy of V. Devecchi.

tolerated.

As evident from Figs. 9 and 15, the analog image usually extends beyond the sampling grid and the acquired image is truncated at the edges of the grid. No information is available about how the signal is distributed outside the grid. This "windowing" effect has consequences on the spatial and temporal spectra of the signal. Their explanation goes beyond the purpose of this tutorial but it implies that it is preferable to have low signals at the edges of the grid. Unfortunately, this condition is not always easy to achieve. As often done in the time domain, the image could be multiplied by a 2D window tapering down at the edges. This would improve the estimate of the spectrum but substantially alter the estimate of the spatial RMS of the EMG and the definition of a "region of activity" of the underlying muscle.

The same considerations discussed above for instantaneous images apply to "RMS images" where the intensity of each pixel does not represent an instantaneous value but the RMS (or other variable) computed over a given time epoch. The spatial sampling and truncation effects may have effects on the represented distribution of muscle activity and be critical in studies concerning compartmentalization or task-specific activation of muscles where details of an image and its spectrum are desirable. Analyses of 2D images of muscles are missing in the literature. This is an open and promising field of research not addressed in this tutorial.

4. Electrode types and location

Although the most widely used sEMG sensors are still two gelled Ag-AgCl pediatric ECG electrodes, other electrode types as well as linear arrays or 2D grids are becoming more and more common in clinical research. Three general types of electrodes can be considered: "wet" (with conductive gel or paste), "dry" (metal-skin contact without gel or paste) and "insulating" (capacitive electrodes) with no electric contact with the skin (Chi et al., 2010; Searle and Kirkup, 2000). They are applied to the skin with a double adhesive layer. Semi-permanent tattoo electrodes are being investigated (Bareket et al., 2016).

Array and grid electrodes allow the implementation of spatial filters with different spatial selectivities (Farina et al., 2003; Mesin, 2018). In these arrangements, the output signal is a linear combination of the monopolar signals detected from the set of electrodes forming the filter. The simplest spatial filter is the set of two electrodes (bipolar detection), described above, whose transfer function is depicted in Fig. 14. Fig. 16a, b, c describe three types of electrodes, a pair, a linear array, and a grid. Fig. 16d, e, f show the power spectrum of three signals simultaneously obtained from three pairs of electrodes with different IED, selected among the contacts of the linear array in Fig. 16b and centered around a central fixed point. The presence of a "dip" is evident in Fig. 16e and f. The frequency of the dips is compatible with a muscle fiber conduction velocity of 4.5 m/s (see Figs. 13 and 14). Spectral dips are usually not so evident because of the spread of the muscle fiber conduction velocity values, mentioned above (Section 3.3).

The sEMG signal and its features depend on a number of factors among which the IED, the location of the electrodes with respect to the innervation zone, and the alignment with the fiber direction, play a very important role (De Nooij et al., 2009; Farina et al., 2002a; Mesin et al., 2009; Nishihara et al., 2010; Rainoldi et al., 2004, 2000; Roy et al., 1986). As a consequence, all features of the signal and the quality of the estimates of muscle fiber conduction velocity depend on the electrode IED and location. Fig. 17 provides a qualitative example of sEMG amplitude changes due to geometrical changes of the biceps brachii. The information obtained from the two pairs of electrodes are contraddictory. While these changes may be attributed, in part, to other reasons, they point out how critical the electrode location with respect to the innervation zone can be (Farina et al., 2002a).

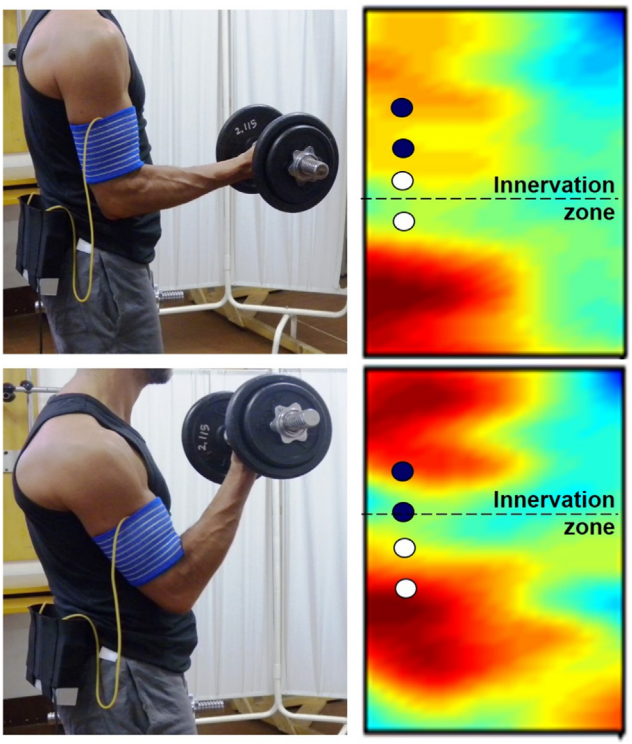

Fig. 17. Example of the effect of muscle shift under a pair of electrodes. Biceps brachii sEMG RMS map (grid of 64 electrodes, IED = 10 mm) during elbow flexion. The images are interpolated. As the muscle shortens the innervation zone shifts upward and the white electrode pair reads a progressively greater signal whereas the black electrode pair reads a progressively smaller one. These opposite changes of amplitude are not necessarily reflecting changes of muscle activity. They mostly reflect a variation of the muscle-electrode geometry (muscle shortening under the electrodes) and may be misleading and misinterpreted. The use of a sEMG map reduces the possibility of misinterpretation. Reproduced from www.robertomerletti.it.

5. Recommendations for best practices

The information contained in the sEMG signal is greatly underexploited. The main purpose of this tutorial is to make current and potential users of sEMG aware of such information content, issues, problems and possible errors associated with the detection and interpretation of this signal. This background knowledge is necessary to understand the signals, assess their quality, process them and interpret the results, allow repetition of a test by others, communicate results and make decisions. The sEMG features of interest may be extracted with different detection techniques:

(1) single channel (to detect sEMG timing, envelope, amplitude and spectral variables),
(2) multiple single channel detection systems on different muscles,
(3) few channels on the same muscle (such as two SD or DD channels to estimate muscle fiber conduction velocity),
(4) linear electrode arrays (to identify the innervation zone and its shifts with movement, fiber length, muscle fiber conduction velocity, optimal position of a single electrode pair),
(5) many channels from an electrode grid (to document compartmentalization of activity, to localize reflex activity, to identify a region of activity, its extension, centroid, etc).

The estimates of sEMG features strongly depend on detection parameters such as electrode size, grid size, IED, electrode location (with respect to the muscle innervation zones) and angle of misalignment of the electrode set with the fiber direction. These parameters may have small or great relevance, depending on the application and purpose of the sEMG detection. When sEMG is detected for the purpose of visualization of muscle activity (e.g. biofeedback) some parameters may be less critical (e.g. electrode size) while they are critical in case of sEMG processing for monitoring myoelectric manifestations of muscle fatigue, studying single motor unit behavior, image compartmentalization, or other analysis (e.g. signal entropy, fractal analysis, wavelet analysis, etc.). For this reason, in any case, detection modalities must be described in clinical reports, theses, manuals, publications and any other form of dissemination and sharing of experience and knowledge, to allow other users to repeat the tests. Users can make their choices, as long as they are repeatable by others, have a rational basis, are well described, justified and reported keeping in mind the considerations mentioned in this tutorial.

5.1. Acquisition of sEMG using a single electrode pair

It is important to point out that the concepts described in Figs. 10–14 apply to both a single electrode pair as well as to a linear electrode array or to a grid. The user must realize that electrode configuration, size and geometry act as filters and modify the shape and the features of the MUAPs. In turn this modifies the features of the interference sEMG in both the time and the frequency domain. The use of different electrode configurations, placements, geometries, makes it impossible to compare signals obtained in different days (e.g. pre-post treatments) or collected by different researchers. For example, two electrode pairs with different IED imply a different detection filter (Fig. 14), a different detection volume, a different sensitivity to cross-talk, a different value of RMS, a different signal power spectrum (Fig. 16), and a different sensitivity to electrophysiological changes in the muscle such as myoelectric manifestations of muscle fatigue (De Luca et al., 2012). Therefore, the chosen IED must be justified. The same applies to electrode size. The location of a pair of electrodes with respect to the innervation zone and to the muscle-tendon junctions of a fusiform muscle parallel to the skin surface, is critical (Farina et al., 2001; Merletti et al., 2003; Rainoldi et al., 2004, 2000) and its choice must be justified. The SENIAM recommendations (Hermens et al., 2000, 1999) provide guidelines that were developed 20 years ago. Considerable additional knowledge has been acquired since then. Just referring to these recommendations is sufficient in many cases but not all. New standardization and education efforts are necessary. Some are under way in the form of consensus papers (Besomi et al., 2019).

The reader is reminded of the fact that the interference pattern of the sEMG is the algebraic sum of the MUAP trains. If the MUAPs shapes are modified by the detection system, the features of the interference pattern observed with one electrode pair (amplitude, power spectrum, fatigue indicators, entropy, etc.) are modified as well (Fig. 12). This may or may not be relevant and is up to the clinician to decide it (e.g. it would not be relevant if only muscle activation intervals were of interest or in biofeedback applications). Some features (signal spatial distribution and intensity, innervation zone shift) are evident in Fig. 17 and will be further discussed in Section 5.2 below.

5.2. Acquisition of sEMG using linear arrays and electrode grids

Instantaneous sEMG images are detected with electrode systems that present three limiting effects that must be considered in clinical research applications because they determine the features of the 1D and 2D sEMG signals in space and time:

(1) the effect of electrode size
(2) the effect of IED
(3) the effect of finite grid size.

These effects have been discussed in (Afsharipour et al., 2019), as well as in Sections 2 and 3 of this tutorial, and provide an update of the

SENIAM indications (Hermens et al., 1999). For example, the IED recommended by SENIAM (20 mm) derived from a compromise between signal amplitude (and therefore Signal/Noise ratio), detection volume and spectral alterations. Because of their importance, these geometrical factors must be reported precisely in order to allow reproduction and comparison of results. Although clinical investigators can make their own choices, they must provide justification for them and demonstrate awareness of the implications.

5.2.1. Electrode size and inter-electrode distance

The electrode size introduces a low-pass filtering effect that attenuates the high frequency components of both the spatial and temporal power spectrum of the sEMG and therefore alters the amplitude and spectral features of the signal (Figs. 11 and 12). This applies to both monopolar and spatially filtered signals (e.g. SD or DD) and to a single electrode pair as well as to a grid of electrodes. The (center-to-center) IED introduces a band-pass filtering effect that combines with the low-pass effect due to the electrode size to give the overall filtering effect depicted in Fig. 14. The filtering applies to SD or DD signals (with different transfer functions) and its time effect depends on the propagation velocity of the APs along the muscle fibers.

Interpolation in space, to reconstruct the spatial distribution of a sEMG feature can be performed only if the Nyquist-Shannon criterion is satisfied. Compromises may be possible in specific situations that should be justified. The impact of these geometrical parameters on the signal and the theoretical reasons for choosing certain values rather than others have been explained in Sections 3 and 4 and are summarized in Table 1.

5.2.2. Grid size

The position of the grid with respect to the muscle(s) of interest must be indicated with respect to anatomical landmarks. The number of electrodes (and of sEMG monopolar channels) of a grid depends on the desired grid size and the selected IED. For example, a grid of 70 mm × 70 mm with IED = e = 10 mm (with electrodes on the edges) requires 64 electrodes, but, if the value e = 5 mm is chosen, the number of electrodes increases to 256 with serious demands on the acquisition system. In addition, it would be desirable to avoid truncation of the sEMG map at the edges of the grid and therefore have low values of sEMG amplitude at the edges to avoid spectral alterations. This is not always possible. The position of the grid with respect to the muscle(s) of interest must be indicated. Interpolated images should not be reported without indication of the original image resolution (IED) and of the interpolation procedure adopted (Fig. 15). In case of small IED values and wet electrodes, particular care must be applied for avoiding conductive paste bridges between nearby contacts.

6. Concluding remarks

The traditional bipolar sEMG detection system is widely applied in clinical research but much less in clinical practice where is mostly used to detect evoked potentials (e.g. to measure nerve conduction velocity). It is a special case of the detection with linear (1D) or grid (2D) array systems, which are even less used. Each of the channels depicted in Figs. 4b, 5b, 6, 8c, d is a classical bipolar recording that provides very partial information about the sEMG image. Further developments in sEMG imaging are under way, just as it happened with X-rays and other imaging techniques. The sEMG images will be one of the inputs to body-machine interfaces and rehabilitation robots. It is important that these developments take place with the participation of the users whose competence in this field must be improved. This is one of the motivations of this tutorial.

It is interesting to notice that some of the literature quoted in this tutorial goes back more than 20 years and a few clinical fundamental articles are more than 40 years old. Nevertheless, they are not well known in the field. The reasons for this slow progress, compared to ECG

Table 1
Ranges of theoretical and compromise values of parameters of a sEMG detection system. "Theoretical values" are those that satisfy the criteria discussed above (Sections 3 and 4). "Compromise values" violate some rule or criterion to a degree such that, for most clinical sEMG applications, the alteration of results is moderate and acceptable. "Other values" may be adopted for noncritical applications but lead to altered sEMG spectra. When mostly muscle activation timing is of interest, these alterations are acceptable.

Geometry or configuration	Theoretical values	Compromise values	Other values for noncritical applications (●)	Notes
Electrode diameter, d	d < 3 mm	3 mm < d < 5 mm	d > 5 mm introduces "smoothing" of the sEMG (low-pass filtering)	See Figs. 11, 12, 14 (Afsharipour et al., 2019; Cattarello et al., 2017; Dimitrova et al., 1999; Farina and Merletti, 2001a,b; Fuglevand et al., 1992)
Inter-electrode distance (IED), e	e < 5–8 mm	8 mm < e < 10 mm	e > 10 mm implies aliasing and introduces "dips" into the spectrum of the SD sEMG altering its features	See Figs. 14, 16 (Afsharipour et al., 2015; Lindstrom and Magnusson, 1977; Lynn et al., 1978; Merletti and Farina, 2016)
Location of a pair of electrodes with respect to the innervation zone	The electrode pair should fit between the innervation zone and a tendon for the entire range of motion being investigated	This may not always be possible for small muscles, even with small IED	Muscle movement under the skin should not bring the innervation zone under the electrode pair	See Fig. 17. This applies to fusiform muscles parallel to the skin (Barbero et al., 2012; Merletti and Farina, 2016)
Alignment with the fiber direction	The electrode pair or array should be aligned with the muscle fiber direction	Misalignments of 15–20° (or more) alter the estimate of amplitude, spectrum and conduction velocity		Merletti et al., 1999b

(●) These values alter the signal, violate the Nyquist-Shannon sampling criterion in space and do not allow interpolation of the images. However, they may be acceptable in specific applications and the authors should justify the irrelevance of the consequences for the specific case.

and EEG, will be discussed elsewhere but should be considered in planning future developments, research and education of users.

This tutorial focuses on very basic and fundamental concepts. It does not address more complex issues such as:

(a) The effect of pennation angle in a plane perpendicular to the skin,
(b) The effect of electrode geometrical parameters of the detection system and 2D spatial filters on sEMG features such as muscle fiber conduction velocity, amplitude and spectral values,
(c) The issues of electrode impedance, interference and noise,
(d) The issue of amplification and conditioning of the sEMG signals.

Some of these issues will be discussed in other tutorials. Clinical applications of any technique require understanding of the physical mechanisms and principles that the technique is based on, and of their limitations. We hope we have contributed to this goal.

Declaration of Competing Interest

The authors declared that there is no conflict of interest.

Acknowledgment

Silvia Muceli was financed by the Life Science Engineering Area of Advance (Chalmers University of Technology) and the European Union's Horizon 2020 research and innovation program under grant agreement number 687795 (project INPUT). The authors are grateful to Prof. D. Farina for his suggestions, to Dr. S. Soedirdjo for preparing Figs. 11, 12, 14 and 15, and to Dr. V. Devecchi for providing Figs. 6 and 16. The authors are very grateful to the three reviewers who provided very extensive and useful suggestions for the improvement of the first version of this work. This tutorial derives, in part, from the teaching material developed within Project CoMES supported by the Laboratory for Engineering of the Neuromuscular System (LISiN, Politecnico di Torino). The CoMES material is freely available on www.roberto-merletti.it as well as on other websites.

References

Afsharipour, B., Soedirdjo, S., Merletti, R., 2019. Two-dimensional surface EMG: the effects of electrode size, interelectrode distance and image truncation. Biomed. Signal Process. Control 49, 298–307. https://doi.org/10.1016/j.bspc.2018.12.001.

Afsharipour, B., Ullah, K., Merletti, R., 2015. Amplitude indicators and spatial aliasing in high density surface electromyography recordings. Biomed. Signal Process. Control 22, 170–179. https://doi.org/10.1016/j.bspc.2015.07.001.

Barbero, M., Merletti, R., Rainoldi, A., 2012. In: Atlas of Muscle Innervation Zones. Springer-Verlag Italia, Milan. https://doi.org/10.1007/978-88-470-2463-2.

Bareket, L., Inzelberg, L., Rand, D., David-Pur, M., Rabinovich, D., Brandes, B., Hanein, Y., 2016. Temporary-tattoo for long-term high fidelity biopotential recordings. Sci. Rep. 6, 25727. https://doi.org/10.1038/srep25727.

Besomi, M., Hodges, P.W., Van Dieën, J., Carson, R.G., Clancy, E.A., Disselhorst-Klug, C., Holobar, A., Hug, F., Kiernan, M.C., Lowery, M., McGill, K., Merletti, R., Perreault, E., Søgaard, K., Tucker, K., Besier, T., Enoka, R., Falla, D., Farina, D., Gandevia, S., Rothwell, J.C., Vicenzino, B., Wrigley, T., 2019. Consensus for Experimental Design in Electromyography (CEDE) project: Electrode selection matrix. J. Electromyogr. Kinesiol. 48, 128–144. https://doi.org/10.1016/j.jelekin.2019.07.008.

Cattarello, P., Soedirdjo, S.D.H., Afsharipour, B., Merletti, R., 2017. Effect of electrode size on amplitude estimation of HDsEMG maps. In: Converging Clinical and Engineering Research on Neurorehabilitation II. pp. 1013–1017. https://doi.org/10.1007/978-3-319-46669-9_164.

Chi, Y.M., Jung, T.P., Cauwenberghs, G., 2010. Dry-contact and noncontact biopotential electrodes: methodological review. IEEE Rev. Biomed. Eng. 3, 106–119. https://doi.org/10.1109/RBME.2010.2084078.

Clancy, E.A., Hogan, N., 1999. Probability density of the surface electromyogram and its relation to amplitude detectors. IEEE Trans. Biomed. Eng. 46, 730–739. https://doi.org/10.1109/10.764949.

De Luca, C.J., Kuznetsov, M., Gilmore, L.D., Roy, S.H., 2012. Inter-electrode spacing of surface EMG sensors: reduction of crosstalk contamination during voluntary contractions. J. Biomech. 45, 555–561. https://doi.org/10.1016/j.jbiomech.2011.11.010.

De Luca, C.J., Merletti, R., 1988. Surface myoelectric signal cross-talk among muscles of the leg. Electroencephalogr. Clin. Neurophysiol. 69, 568–575. https://doi.org/10.1016/0013-4694(88)90169-1.

De Nooij, R., Kallenberg, L.A.C., Hermens, H.J., 2009. Evaluating the effect of electrode location on surface EMG amplitude of the m. erector spinae p. longissimus dorsi. J. Electromyogr. Kinesiol. 19, e257–e266. https://doi.org/10.1016/j.jelekin.2008.03.013.

Dimitrova, N.A., Dimitrov, G.V., Chihman, V.N., 1999. Effect of electrode dimensions on motor unit potentials. Med. Eng. Phys. 21, 479–485. https://doi.org/10.1016/S1350-4533(99)00069-7.

Farina, D., Arendt-Nielsen, L., Merletti, R., Indino, B., Graven-Nielsen, T., 2003. Selectivity of spatial filters for surface EMG detection from the tibialis anterior muscle. IEEE Trans. Biomed. Eng. 50, 354–364. https://doi.org/10.1109/TBME.2003.808830.

Farina, D., Cescon, C., Merletti, R., 2002a. Influence of anatomical, physical, and detection-system parameters on surface EMG. Biol. Cybern. 86, 445–456. https://doi.org/10.1007/s00422-002-0309-2.

Farina, D., Merletti, R., 2001a. A novel approach for precise simulation of the EMG signal detected by surface electrodes. IEEE Trans. Biomed. Eng. 48, 637–646. https://doi.org/10.1109/10.923782.

Farina, D., Merletti, R., 2001b. Effect of electrode shape on spectral features of surface detected motor unit action potentials. Acta Physiol. Pharmacol. Bulg. 26, 63–66.

Farina, D., Merletti, R., Indino, B., Nazzaro, M., Pozzo, M., 2002b. Surface EMG crosstalk between knee extensor muscles: experimental and model results. Muscle Nerve 26, 681–695. https://doi.org/10.1002/mus.10256.

Farina, D., Merletti, R., Nazzaro, M., Caruso, I., 2001. Effect of joint angle on EMG variables in leg and thigh muscles. IEEE Eng. Med. Biol. Mag. 20, 62–71. https://doi.org/10.1109/51.982277.

Farina, D., Mesin, L., Martina, S., Merletti, R., 2004. A surface EMG generation model with multilayer cylindrical description of the volume conductor. IEEE Trans. Biomed. Eng. 51, 415–426. https://doi.org/10.1109/TBME.2003.820998.

Fuglevand, A.J., Winter, D.A., Patla, A.E., Stashuk, D., 1992. Detection of motor unit action potentials with surface electrodes: influence of electrode size and spacing. Biol. Cybern. 67, 143–153. https://doi.org/10.1007/BF00201021.

Gootzen, T.H., 1990. Muscle Fibre and Motor Unit Action Potentials. A biophysical basis for clinical electromyography. University of Nijmegen (NL) Thesis.

Griep, P.A.M., Boon, K.L., Stegeman, D.F., 1978. A study of the motor unit action potential by means of computer simulation. Biol. Cybern. 30, 221–230. https://doi.org/10.1007/BF00361043.

Helal, J., Bouissou, P., 1992. The spatial integration effect of surface electrode detecting myoelectric signal. IEEE Trans. Biomed. Eng. 39, 1161–1167. https://doi.org/10.1109/10.168695.

Hermens, H.J., Freriks, B., Disselhorst-Klug, C., Rau, G., 2000. Development of recommendations for SEMG sensors and sensor placement procedures. J. Electromyogr. Kinesiol. 10, 361–374. https://doi.org/10.1016/S1050-6411(00)00027-4.

Hermens, H.J., Freriks, B., Merletti, R., Stegeman, D., Blok, J., Rau, G., Disselhorst-Klug, C., Hägg, G., 1999. European Recommendations for Surface Electromyography Results of the SENIAM Project. Roessingh Research and Development, Enschede.

Lindstrom, L.H., Magnusson, R.I., 1977. Interpretation of myoelectric power spectra: a model and its applications. Proc. IEEE 65, 653–662. https://doi.org/10.1109/PROC.1977.10544.

Lowery, M.M., Stoykov, N.S., Taflove, A., Kuiken, T.A., 2002. A multiple-layer finite-element model of the surface EMG signal. IEEE Trans. Biomed. Eng. 49, 446–454. https://doi.org/10.1109/IEMBS.2001.1020369.

Lynn, P.A., Bettles, N.D., Hughes, A.D., Johnson, S.W., 1978. Influence of electrode geometry on bipolar recordings of the surface electromyogram. Med. Biol. Eng. Comput. 16, 651–660. https://doi.org/10.1007/BF02442444.

Malmivuo, J., Plonsey, R., 1995. Bioelectromagnetism: Principles and Applications of Bioelectric and Biomagnetic Fields. Oxford University Press.

Merletti, R., Afsharipour, B., Piervirgili, G., 2013. High density surface EMG technology, Converging Clinical and Engineering Research on. Neurorehabilitation 1205–1209. https://doi.org/10.1007/978-3-642-34546-3_199.

Merletti, R., Farina, D., 2016. In: Surface Electromyography: Physiology, Engineering, and Applications. John Wiley & Sons, Hoboken, NJ. https://doi.org/10.1002/9781119082934.

Merletti, R., Farina, D., Gazzoni, M., 2003. The linear electrode array: a useful tool with many applications. J. Electromyogr. Kinesiol. 13, 37–47. https://doi.org/10.1016/S1050-6411(02)00082-2.

Merletti, R., Lo Conte, L., Avignone, E., Guglielminotti, P., 1999a. Modeling of surface myoelectric signals - Part I: Model implementation. IEEE Trans. Biomed. Eng. 46, 810–820. https://doi.org/10.1109/10.771190.

Merletti, R., Roy, S.H., Kupa, E., Roatta, S., Granata, A., 1999b. Modeling of surface myoelectric signals - Part II Model-based signal interpretation. IEEE Trans. Biomed. Eng. 46, 821–829. https://doi.org/10.1109/10.771191.

Mesin, L., 2018. Optimal spatio-temporal filter for the reduction of crosstalk in surface electromyogram. J. Neural Eng. 15, 016013. https://doi.org/10.1088/1741-2552/aa8f03.

Mesin, L., Farina, D., 2004. Simulation of surface EMG signals generated by muscle tissues with inhomogeneity due to fiber pinnation. IEEE Trans. Biomed. Eng. 51, 1521–1529. https://doi.org/10.1109/TBME.2004.827551.

Mesin, L., Merletti, R., Rainoldi, A., 2009. Surface EMG: the issue of electrode location. J. Electromyogr. Kinesiol. 19, 719–726. https://doi.org/10.1016/j.jelekin.2008.07.006.

Nazarpour, K., Al-Timemy, A.H., Bugmann, G., Jackson, A., 2013. A note on the probability distribution function of the surface electromyogram signal. Brain Res. Bull. 90, 88–91. https://doi.org/10.1016/j.brainresbull.2012.09.012.

Nishihara, K., Chiba, Y., Suzuki, Y., Moriyama, H., Kanemura, N., Ito, T., Takayanagi, K., Gomi, T., 2010. Effect of position of electrodes relative to the innervation zone on-surface EMG. J. Med. Eng. Technol. 34, 141–147. https://doi.org/10.3109/03091900903480754.

Rainoldi, A., Melchiorri, G., Caruso, I., 2004. A method for positioning electrodes during surface EMG recordings in lower limb muscles. J. Neurosci. Methods 134, 37–43. https://doi.org/10.1016/j.jneumeth.2003.10.014.
Rainoldi, A., Nazzaro, M., Merletti, R., Farina, D., Caruso, I., Gaudenti, S., 2000. Geometrical factors in surface EMG of the vastus medialis and lateralis muscles. J. Electromyogr. Kinesiol. 10, 327–336. https://doi.org/10.1016/S1050-6411(00)00024-9.
Roeleveld, K., Blok, J.H., Stegeman, D.F., van Oosterom, A., 1997. Volume conduction models for surface EMG; confrontation with measurements. J. Electromyogr. Kinesiol. 7, 221–232. https://doi.org/10.1016/S1050-6411(97)00009-6.
Rosenfalck, P., 1969. Intra and extracellular fields of active nerve and muscle fibers. A physico-mathematical analysis of different models. Acta Physiol. Scand. 321, 1–168.
Roy, S.H., De Luca, C.J., Schneider, J., 1986. Effects of electrode location on myoelectric conduction velocity and median frequency estimates. J. Appl. Physiol. 61, 1510–1517. https://doi.org/10.1152/jappl.1986.61.4.1510.
Searle, A., Kirkup, L., 2000. A direct comparison of wet, dry and insulating bioelectric recording electrodes. Physiol. Meas. 21, 271–283. https://doi.org/10.1088/0967-3334/21/2/307.
Stegeman, D.F., Blok, J.H., Hermens, H.J., Roeleveld, K., 2000. Surface EMG models: properties and applications. J. Electromyogr. Kinesiol. 10, 313–326. https://doi.org/10.1016/S1050-6411(00)00023-7.
Urbanek, H., van der Smagt, P., 2016. iEMG: Imaging electromyography. J. Electromyogr. Kinesiol. 27, 1–9. https://doi.org/10.1016/j.jelekin.2016.01.001.
Vieira, T.M., Botter, A., Muceli, S., Farina, D., 2017. Specificity of surface EMG recordings for gastrocnemius during upright standing. Sci. Rep. https://doi.org/10.1038/s41598-017-13369-1.

Prof. Roberto Merletti graduated in Electronics Engineering from Politecnico di Torino, Italy, and obtained his M.Sc. and PhD in Biomedical Engineering from the The Ohio State University. He has been Associate Professor of Biomedical Engineering at Boston University were he was also Research Associate at the NeuroMuscular Research Center. He has been Full Professor of Biomedical Engineering at Politecnico di Torino where he established, in 1996, the Laboratory for Engineering of the Neuromuscular System (LISiN) of which he has been Director up to 2015. He has trained at LISIN more than 70 researcher (15 doctoral students) from various countries.

His research activity covers basic investigation of sEMG, applications in prevention, rehabilitation, ergonomics, and sport. This activity led to over 200 peer reviewed publications and four textbooks.

He is Senior Member of IEEE, Fellow of ISEK, and member of the Editorial Board of three international journals. His e-mail is roberto.merletti@formerfaculty.polito.it and his personal web site is http://www.robertomerletti.it which has a strong teaching connotation.

Silvia Muceli is a Marie Curie Fellow and Assistant Professor in Life Science Engineering at Chalmers University of Technology, Gothenburg, Sweden. She received her MSc in Electronics Engineering from the University of Cagliari, Italy, in 2007, and PhD in Biomedical Science and Engineering from Aalborg University, Denmark, in 2013. She worked at the University Medical Center Göttingen, Georg-August University, Germany (2011-2017), until she moved to Imperial College London, UK, to work as a research associate at the Department of Bioengineering (2017-2019). Her main research interests include surface and intramuscular electromyography, biomedical signal processing and modelling, bioelectrode design, neurophysiology of movement, sensorimotor development, and advanced prosthetic control.